Accepted Manuscript

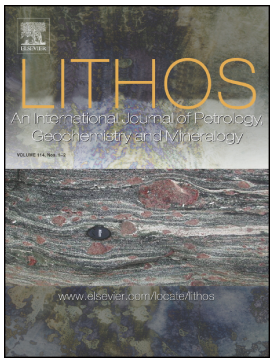

The petrogenesis and tectonic significance of the early cretaceous intraplate granites in eastern China: The Laoshan granite as an example

Yajie Gao, Yaoling Niu, Meng Duan, Qiqi Xue, Pu Sun, Shuo Chen, Yuanyuan Xiao, Pengyuan Guo, Xiaohong Wang, Yanhong Chen

PII: S0024-4937(19)30051-9
DOI: https://doi.org/10.1016/j.lithos.2019.01.031
Reference: LITHOS 4961

To appear in: *LITHOS*

Received date: 3 October 2018
Accepted date: 24 January 2019

Please cite this article as: Y. Gao, Y. Niu, M. Duan, et al., The petrogenesis and tectonic significance of the early cretaceous intraplate granites in eastern China: The Laoshan granite as an example, LITHOS, https://doi.org/10.1016/j.lithos.2019.01.031

This is a PDF file of an unedited manuscript that has been accepted for publication. As a service to our customers we are providing this early version of the manuscript. The manuscript will undergo copyediting, typesetting, and review of the resulting proof before it is published in its final form. Please note that during the production process errors may be discovered which could affect the content, and all legal disclaimers that apply to the journal pertain.

ACCEPTED MANUSCRIPT

The petrogenesis and tectonic significance of the Early Cretaceous intraplate granites in eastern China: the Laoshan granite as an example

Yajie Gao[1,2,3*], Yaoling Niu[1,2,4,5*], Meng Duan[5], Qiqi Xue[5], Pu Sun[1], Shuo Chen[1], Yuanyuan Xiao[1], Pengyuan Guo[1], Xiaohong Wang[1], Yanhong Chen[5]

[1] Institute of Oceanology, Chinese Academy of Sciences, Qingdao 266071, China

[2] Laboratory for Marine Geology, Qingdao National Laboratory for Marine Science and Technology, Qingdao 266061, China

[3] University of Chinese Academy of Sciences, Beijing 100049, China

[4] Department of Earth Sciences, Durham University, Durham DH13LE, UK

[5] School of Earth Science and Resources, China University of Geosciences, Beijing 100083, China

 Corresponding authors at:

Institute of Oceanology, Chinese Academy of Sciences, Qingdao 266071, China.

ocean.gao@foxmail.com (Y. Gao), yaoling.niu@durham.ac.uk (Y. Niu).

ACCEPTED MANUSCRIPT

ACCEPTED MANUSCRIPT

Abstract

The Laoshan granite is an example of the widespread intraplate granitoids of early Cretaceous age in eastern continental China. The petrogenesis of these granitoids remains in dispute and we choose the Laoshan granite as the representative case to study these granitoids. Zircons from the Laoshan granite give a crystallization age of ~120 Ma, which is consistent with the emplacement age of ~ 126 Ma given by the bulk-rock Rb-Sr isochron. Representative samples from the granite show a large range of major element compositional variation (e.g., SiO_2/MgO = 64 to 1937), reflecting a varying degree of fractional crystallization of plagioclase, alkali feldspar, amphibole, biotite and accessory phases as observed. The samples are enriched in light rare earth elements, Rb, Th and U, but depleted in Ba and Sr with negative Eu anomalies. The high $^{87}Sr/^{86}Sr$ (0.7083 to 1.2265) is largely caused by variably high Rb/Sr (~ 0.31 to 91 with an average of ~ 13) due to feldspar fractionation. The low $\varepsilon_{Nd}(t)$ (−13.8 to −19.5), $\varepsilon_{Hf}(t)$ (−14.6 to −24.4), and $(^{206}Pb/^{204}Pb)_i$ (16.244 to 17.304) are consistent with significant contributions of the lower continental crust to magmas parental to the Laoshan granite. The origin of the parental magmas is best understood as resulting from anatexis of the lower crust (~20% - 25% partial melting of the mafic granulite) triggered by and mixed with the underplating and intruding basaltic magmas. The basaltic magmas were likely derived from melting of the thinning lithosphere being transformed into the asthenosphere as the result of “basal hydration weakening” with the water ultimately coming from dehydration of the stagnant paleo-Pacific slab in the mantle transition zone.

ACCEPTED MANUSCRIPT

Key words: **eastern China; early Cretaceous; intra-plate; paleo-Pacific plate; basal hydration weakening**

ACCEPTED MANUSCRIPT

ACCEPTED MANUSCRIPT

1 Introduction

The Cretaceous Laoshan granite is one of the widespread Mesozoic granitoid intrusions in eastern continental China (Fig.1a). The petrogenesis of these granitoids is thought to be related to the paleo-Pacific plate subduction, but debate continues on actual mechanisms (Jahn et al., 1999; Li et al., 2014; Wang et al., 1995, 2001; Wu et al., 2002; Zhou and Li, 2000; Zhou et al., 2006). Niu et al. (2015) argued that all of the Jurassic-Cretaceous granitoids in the interiors of eastern continental China are of intraplate origin genetically associated with the lithosphere thinning beneath the region through basal hydration weakening (Niu, 2005) with the water ultimately coming from dehydration of the paleo-Pacific plate lying stagnant in the mantle transition. To test this hypothesis, we focus on the petrology and geochemistry of the Laoshan granite, which is on the east coast of continental China but was emplaced within the continental interiors in the Mesozoic (Niu et al., 2015; Niu and Tang, 2016; Tang et al., 2016). There are several studies on the Laoshan granite, but the petrogenesis is still controversial (Yan and Shi, 2014; Wei, 2008; Zhao et al., 1997). These authors mainly focus on the problematic A-type classification that overlaps with highly evolved I-type granitoids (Chappell and White, 2001; King et al., 1997; Whalen et al., 1987). In this paper, we report the results of our detailed petrological, geochronological and geochemical study on the Laoshan granite and discuss its petrogenesis, which offers an effective test on the hypothesis by Niu et al. (2015) as mentioned above.

ACCEPTED MANUSCRIPT

2 Geological background and Petrography

The Laoshan granite is located in the Jiaodong Peninsula on the east coast of continental China (Fig. 1). Three episodes (i.e., Triassic, Jurassic, and Cretaceous) of Mesozoic magmatism are recognized in the Jiaodong Peninsula (Guo et al., 2005; Goss et al., 2010; Liu et al., 2008; Yang et al., 2005a, 2005b; Zhao et al., 2017; Fig. 1b). The Cretaceous mafic rocks include the Jimo basalts and numerous mafic dikes of 130-67 Ma age (Cai et al., 2015; Liang et al., 2017; Ma et al., 2014, 2016; Yang et al., 2005a, 2005b; Ying et al., 2006; Zhang et al., 2011; Zhang et al., 2012). The Laoshan pluton is an early Cretaceous granitoid intrusion, which is termed the Laoshan granite for discussion convenience. It is exposed in an area of ~ 600 km^2 (Fig. 1c) and belongs to the 500 km long so-called Early Cretaceous A-type granite belt (from Taolin in Jiangsu, towards NEE, to Rizhao, Jiaonan, Qingdao, Laoshan, Haiyang, Rushan, and Weihai; Wang et al., 1995). It intruded the Cretaceous volcanic, Jurassic-Cretaceous sedimentary and Precambrian metamorphic rocks of the Jiaonan group (Fig. 1c). Our samples include monzogranite, syenogranite and alkali-feldspar granite in terms of modal mineralogy and the petrographic details (Table 1). The samples are light grey to pink in color and medium to fine in grain size. Most of the samples are relatively uniform with mafic magmatic enclaves (MMEs) present in places (e.g., QD15-03; Fig.2A). Both the MMEs and host have the same mineralogy but the MMEs have greater modal amphibole and biotite. The main mineral phases of monzogranites (Fig.2B) are feldspar, plagioclase and quartz. The alkali-feldspar granite (Fig.2C) is dominated by alkali-feldspar and quartz. The alkali feldspars are mainly perthitic potassium feldspar. Mafic minerals (1%~10%) are biotite and amphibole. Mafic alkali minerals like aegirine (Zhao et al., 1997) is not observed in our

ACCEPTED MANUSCRIPT

samples. Accessory phases (< 1%) include apatite, sphene, magnetite, zircon and fluorite (Fig.2D).

3 Analytical methods

3.1 Zircon U-Pb dating

Zircon separation was done in the Laboratory of the Langfang Institute of Regional Geological Survey using a combined method of heavy liquid, magnetic and manual selection under a binocular. The selected zircons were set in an epoxy mount before polished to expose zircon interiors. Cathodoluminescence(CL)images were taken at Beijing GeoAnalysis CO. Ltd to examine the internal structure of individual zircon grains needed for spot analysis. Zircon U-Pb dating was done using LA-ICP-MS in the Ocean Lithosphere and Mantle Dynamics Laboratory, Institute of Oceanology, Chinese Academy of Sciences (OLMDL-IOCAS). We used an Agilent 7900 ICP-MS instrument coupled with 193 nm Photon Machines Excite Laser for analysis. Helium was applied as a carrier gas. The laser spot size was 35 μm. Zircon 91500 was used as the external standard for U-Pb dating (Wiedenbeck et al., 1995), and analyzed twice between every five unknowns. NIST 610 glass was used as an external standard for trace element analysis (Xiao et al., unpublished). The age calculation was done using the method of Liu et al. (2010) and the Concordia diagrams were plotted using Isoplot (Ludwing, 2003).

3.2 Major and trace elements

The bulk-rock major and trace element analysis was done in OLMDL-IOCAS. Bulk-rock major elements were analyzed using Agilent 5100 ICP-OES following the method of Kong et al.

ACCEPTED MANUSCRIPT

(unpublished). Trace element analysis was done using ICP-MS (Agilent 7900) following Chen et al. (2017). The bulk-rock major (Appendix 1) and trace (Appendix 2) elements of USGS reference materials analyzed together with our samples agree well with reference values within error (GeoREM, http://georem.mpch-mainz.gwdg.de/).

3.3 Bulk-rock Sr-Nd-Pb-Hf isotopes

Bulk-rock Sr-Nd-Pb-Hf isotopes analysis was done in the Radiogenic Isotope Facility at the University of Queensland, Australia. The rock powders were dissolved in a mixture of double-distilled concentrated HNO_3 and HF, and dried on a hot plate at 80°C. After converting any fluoride to nitrate, the dried residue was dissolved with 3 ml 2N HNO_3 and 1.5 ml was loaded onto a stack of Sr-spec, Thru-spec and LN-spec resin columns to separate Sr, Nd, Pb, and Hf from the matrix, using a streamlined procedure modified after Míková and Denková (2007) and Yang et al. (2010).

All the measured $^{87}Sr/^{86}Sr$, $^{143}Nd/^{144}Nd$, $^{176}Hf/^{177}Hf$ ratios were normalized to $^{86}Sr/^{88}Sr$ = 0.1194, $^{146}Nd/^{144}Nd$= 0.7219 and $^{179}Hf/^{177}Hf$=0.7325, respectively. Analyses of NBS987 standard run during the same period gave $^{87}Sr/^{86}Sr$=0.710249±9 (n=22, 2σ). In the course of $^{143}Nd/^{144}Nd$ and $^{176}Hf/^{177}Hf$ analysis, the in-house Nd standard, Ames Nd Metal and 10 ppm Hf ICP solution from Choice Analytical were used as instrument drift monitors, respectively. This in-house Nd Metal and Hf standards were cross-calibrated against the JNdi-1 Nd international standard and the JMC-475 Hf international standard, respectively. Analyses of in-house Nd standard gave $^{143}Nd/^{144}Nd$= 0.511965±6 (n=12, 2σ). Analyses of in-house Hf standard yielded a mean $^{176}Hf/^{177}Hf$ of 0.282147±5 (n=39, 2σ). Pb isotope ratios were normalized for instrumental mass

ACCEPTED MANUSCRIPT

fraction relative to NBS/SRM 997 $^{203}Tl/^{205}Tl$ = 0.41891, which were then normalized against NBS981 (see Sun et al., 2017). The values of USGS reference materials run with our samples are given in Appendix 3, which agree with the reference values (GeoREM, http://georem.mpch-mainz.gwdg.de/). Procedures for Sr, Nd, Pb and Hf elemental column separation and analytical details are given in Guo et al. (2014) and Sun et al. (2017).

4 Results

4.1 Zircon U-Pb ages

Zircons from LS15-15 and QD15-22 have been dated (Table 2). The zircons are mostly euhedral, transparent, ranging from 100 to 200 μm in size with length-to-width ratios of 1:1 - 2:1. The cathodoluminescence (CL) images show oscillatory zoning of magmatic origin. The zircons have varying U (48.46 to 439.44 ppm) and Th (105.83 to 723.63 ppm) concentrations with varied Th/U ratio of 0.94 - 2.18. After rejecting discordant analyses, we obtain zircon crystallization age of ~ 120 Ma within error (Fig. 3). This age is similar to the youngest ages of the granitoids in the region (Fig. 1; Guo et al., 2005; Goss et al., 2010). Captured zircon cores exist in both samples, plot along or close to the Concordia. Their age is around 140~130 Ma (Table 2), similar to the ages of Cretaceous granitoids in the region (Guo et al., 2005).

4.2 Bulk-rock major and trace elements

4.2.1 Major elements

The samples (Fig. 4) are compositionally alkali rich ($Na_2O + K_2O$ = 7.82 ~ 10.63 wt.%) and calc-alkaline (Rittmann Serial Indexσ [= $(K_2O+Na_2O)^2$ / (SiO_2-43), units in wt.%] < 9; in

ACCEPTED MANUSCRIPT

Appendix 6) without excess alkalis (A/NK > 1; Fig. 4). Previous classification of the Laoshan granite is largely based on SiO_2 content (Fig. 4; Yan and Shi, 2014). The so-called A-type granites are actually highly evolved ones with high SiO_2 (Fig.4) and low Al_2O_3 (Fig. 5). Our samples span a larger range of SiO_2 than the data in the literature (Yan and Shi, 2014). Thus, the changes in alkali content between the I-type granite and the A-type granite in the literature can be observed (Fig.4). The changes of samples in alkali content was most likely controlled by fractional crystallization in consistence with the petrography. Because the liquidus temperature is inversely correlated with SiO_2 but positively correlated with MgO during magma evolution, the ratio of SiO_2/MgO can be an effective parameter to describe the extent of magma differentiation (see Fig. 5). For example, magma cooling and mineral crystallization lead to increasing SiO_2/MgO in the residual melts. Thus, the most evolved granite experienced highest extent of crystallization and thus have the highest SiO_2/MgO. Note that by using the combined parameter SiO_2/MgO, we emphasize that these samples represent products of varying extent of fractional crystallization (Fig.5) despite the fact that the granitoid rocks are not pure liquids, but mixtures of liquids with incompletely segregated crystals (both liquidus and residual phases).

4.2.2 Trace elements

Fig. 6a shows chondrite-normalized rare earth element (REE) patterns of the samples. They are enriched in light REEs (Appendix 6, Fig. 6a) and have varying negative Eu anomalies (Eu/Eu*=0.05–0.77, Fig. 7a). Four samples have low abundances from Sm to Tm, which can also be found in some highly fractional granites (Fig. 6, Qiu et al., 2008). Fig. 6b shows that the samples are enriched in Rb, Th and U, but depleted in Ba and Sr. This is consistent with the

ACCEPTED MANUSCRIPT

negative Eu anomalies due to feldspar fractionation. Like most granites, our samples are characteristically depleted in Nb, Ta and Ti. The P depletion results from apatite fractionation.

4.3 Bulk-rock Sr-Nd-Pb-Hf isotopes

Bulk-rock Sr-Nd-Pb-Hf isotopic data are given in Appendix 7. The $\varepsilon_{Nd}(t)$, $\varepsilon_{Hf}(t)$, $(^{206}Pb/^{204}Pb)_i$, $(^{207}Pb/^{204}Pb)_i$ and $(^{208}Pb/^{204}Pb)_i$ are calculated at 120Ma. Samples have variably high $^{87}Sr/^{86}Sr$ (0.7083 to1.2265; Fig. 7b) because of feldspar fractionation-reduced low Sr in the samples, hence the high Rb/Sr and high radiogenic ^{87}Sr as manifested by the correlated negative Sr/Sr* and Eu/Eu* anomalies (Fig. 7a; Halliday et al., 1991; Sallet et al., 2000; Shao et al., 2015). Calculation of initial $^{87}Sr/^{86}Sr$ for such high Rb/Sr samples would become problematic (Cavazzini, 1994; Mahood and Halliday, 1988; Sallet et al., 2000), but the bulk-rock isochron gives a unique initial $^{87}Sr/^{86}Sr$ = 0.7061 and significant isochron age of ~126 Ma (Fig. 7b), representing the magma emplacement age and is consistent with the zircon crystallization ages (Fig. 3; also see section 5.3). Our samples have enriched $\varepsilon_{Nd}(t)$ (−13.8 to −19.5) and $\varepsilon_{Hf}(t)$ (−14.6 to −24.4), defining a trend that is on the extension of the mantle array (Fig. 8). Both Nd-Hf and Pb isotopes ($(^{206}Pb/^{204}Pb)_i$ = 16.244 to 17.304) indicate a trend of magma mixing, with the enriched endmember and the less enriched endmember (Fig. 8, Fig.9).

5 Discussion

5.1 Intra-plate setting

Previous studies (Zhao et al., 1997) used the tectonic discrimination plots to classify the calc-alkali granites into volcanic arc granite (VAG) and within plate granite (WPG). Here we

ACCEPTED MANUSCRIPT

emphasize that the intra-plate tectonic setting of Laoshan granites in Mesozoic is already known (see above and below). It is thus unnecessary to use tectonic discrimination plots to interpret tectonic settings that are geologically incorrect. The Korean Peninsula has long been thought to be part of the North China Craton (once called Sino-Korean para-platform) with similar Precambrian basement (Zhai et al., 2005, 2007, 2016). Recent studies have been able to correlate the lithologies between the Jiaodong Peninsula and the Korean Peninsula (Hu et al., 2012; Oh and Kusky, 2007; Zhai et al., 2005, 2007, 2016). Besides, the paleomagnetic data analysis (Zhao et al., 1999), the combined method of seismic tomography and gravity data (Hu et al., 2012) confirm the traditional view. That is, the North China Craton and the Korean Peninsula have been a single coherent block since the early Paleozoic. However, how the Jiaodong Peninsula and Korean Peninsula may have actually correlated has not been explained until recently when Niu and Tang (2016) and Tang et al. (2016) elaborated the origin of the Yellow Seas as a continent-rifted basin since ~ 56 Ma. This means the Laoshan granite was emplaced in an intra-plate setting before the opening of the Yellow Sea. This is consistent with the contemporaneous granitoid magmatism in the Russian Far East (as young as ~ 56 Ma), South Korea and Southwest Japan (as young as 71 Ma; Tang et al., 2016).

5.2 Origin of the Laoshan granite

Several models have been proposed for the origin of the Laoshan granite in the literature, including (1) partial melting of residual basaltic lower crust that had been previously melted to produce I-type granites (Zhao et al., 1997), (2) low degree melting of intermediate to felsic lower crust under granulite facies (Wei, 2008), and (3) mixing of the asthenosphere-derived basaltic melt and the lower continental crust - derived melt (Yan and Shi, 2014). We evaluate these scenarios

ACCEPTED MANUSCRIPT

and propose our explanation that is consistent with the geological, petrological and geochemical data.

5.2.1 Assessing the model of lower continental crust anatexis

Several experimental studies on partial melting of intermediate to felsic crustal rocks (Skjerlie and Johnston, 1992; Patiño Douce, 1997) have been proposed to explain the origin of granite similar to the Laoshan granite with high $^{T}Fe_2O_3$, K_2O and low Al_2O_3, CaO, MgO, Sr, and Eu. All the existing models (Zhao et al., 1997; Wei, 2008; Yan and Shi, 2014) require melting of the lower continental crust for magmas parental to the Laoshan granite. Thus, it is necessary to test whether melting of the mafic lower continental crust can indeed produce magmas parental to the Laoshan granite. To quantify and assess the partial melting interpretation, we choose a mafic granulite (90DA1, SiO_2 = 51.6 wt.%, MgO = 10.8 wt.%; Na_2O+K_2O = 2.52 wt.%; Zhou et al. 2002) and the average composition of the granulite of the Yangtze craton (YC-LCC, SiO_2 = 65.7 wt.%, MgO = 2.3 wt.%; Gao et al., 1998) as the source rocks to model partial melting of the mafic and intermediate lower continental crust separately. The MELTS (Ghiorso and Sack, 1995) used for the model is set at 10 kbars with the temperature range of 1200-700°C at 20K intervals (Fig. 10d). The calculation shows that 20% - 28% partial melting of the mafic granulite can produce melts that match the least evolved (low SiO_2/MgO) composition of the Laoshan granite (Fig.10d). This corresponds to temperature condition of 900-1040°C, consistent with the least evolved compositions of the Laoshan granite. Varying extents of fractional crystallization from such least evolved samples can effectively explain the entire data range (e.g., SiO_2/MgO) of the Laoshan granite. This is consistent with the major and trace element data as discussed below. Obviously,

ACCEPTED MANUSCRIPT

melting of the intermediate or felsic YC-LCC cannot produce melts parental to the Laoshan granite. This model provides a conceptual clue to the feasibility of mafic crustal melting and provides clue to the hypothesis of lower continental crust melting for the granitoids in the continental interiors (Niu et al.,2015).

5.2.2 Constraints on the source

The model above shows that magmas parental to the Laoshan granite can be generated by anatexis of the lower continental crust, which is consistent with isotope data. The isotope compositions of the lower crust beneath the Jiaodong Peninsula vary greatly (Fig.8; Jahn et al., 2008), and some values coincide with the Laoshan granite. In other words, some samples can be formed directly through anatexis. The lower continental crust with a normal geothermal gradients is seldom able to melt and anatexis requires excess heat source (e.g., Huppert and Sparks, 1988). Although minor volumes of partial melt can be produced by fluid-present melting at high water fugacity (Bergantz, 1989), because the Laoshan granitoid magmatism occurred in an "intra-plate" setting away from any known paleo-subduction zone (Fig. 11), the excess heat required for the anatexis must have come from mantle-derived basaltic melts (Niu, 2005; Niu et al., 2015; Zhou et al., 2006). Isotopically, the $\varepsilon_{Nd}(t)$ (−13.8 to −19.5) and $\varepsilon_{Hf}(t)$ (−14.6 to −24.4) values (Fig. 8) of the Laoshan granite lie between the range of the lower crust of the Jiaodong Peninsula (Jahn et al. 2008) and the Mesozoic lithospheric mantle-derived melts (basalts from Guo et al., 2013; dolerite from Liang et al., 2017). The isotopic range of samples provide evidence for the crustal anatexis induced by mantle-derived basaltic melts. That is, the basaltic melts not only provide the heat but also contribute material to the Laoshan granite magmatism. This observation supports the

ACCEPTED MANUSCRIPT

hypothesis of lower continental crust melting for the intra-plate granitoids (Niu et al.,2015; also see section 5.2.1 and section 5.2.3 below).

The question then concerns the origin of the basaltic melts. Among the several ideas (see section 5.3) about the mechanism of widespread lithosphere thinning throughout entire eastern China in the Mesozoic (Niu, 2005, 2014; Niu et al., 2015), the physically most likely process is the basal hydration weakening. That is, the lithosphere was being thinned by converting the basal portions of the lithosphere into the asthenosphere, accompanied by partial melting and basaltic magmatism (Niu, 2005, 2006, 2009, 2014; Niu et al., 2015). Niu (2014) suggested that basaltic melts are most likely to have been derived from being-hydrated and -thinned lithosphere with the water coming from the paleo-Pacific plate lying stagnantly in the mantle transition zone. The ascent, intruding and underplating of the basaltic magmas provide the heat for the widespread crustal melting for the intra-plate granitoid magmatism in eastern China (Niu et al., 2015).

Some studies (Yan and Shi, 2014; Zhao et al., 2017) suggested the upper continental crust as a candidate of the magma source, but this is not the case for the Laoshan granite. Because the basaltic melts required to provide the heat first encounter the deep crust to cause its melting, which prevents upper crustal melting. Upper crustal magma contamination is possible during magma ascent, but not the primary source.

5.2.3 The magma mixing model

As discussed above, we propose that the lithospheric mantle-derived basalts provide both heat and material for the primary magmas parental to the Laoshan granite. To quantitatively estimate the relative contributions of the lithosphere mantle-derived melts and the lower continental crust,

ACCEPTED MANUSCRIPT

we used the average Nd isotope composition of the Mesozoic lithospheric mantle-derived melts in the Jiaodong Peninsula (basalts from Guo et al., 2013; dolerite from Liang et al., 2017) as the less enriched endmember, and the highest Nd isotope value of the lower continental crust of the Jiaodong Peninsula (Jahn et al., 2008) as the enriched endmember for binary isotope mixing calculation. The calculations show the significant contribution of the lower continental crust. This mixing calculation using Nd-Hf isotopes is conceptually illustrative on the significance of crustal melting induced by lithosphere-derived basaltic melts in the Mesozoic although the exact mass contributions cannot be constrained because of the two isotopic end-members cannot be well constrained.

Our petrological modeling by lower continental crust anatexis (Fig.10d) shows that ~ 7% - 27% partial melting of the mafic granulite with 10% contribution of mantle-derived basaltic melts (Liang et al., 2017) can produce melts that match the least evolved (low SiO_2/MgO) composition of the Laoshan granite. Hence, with all the uncertainties considered, ~ 20% – 25% melting of the mafic lower crust heated by and mixed with ~ 10% lithosphere-derived basaltic melts can explain the data. Varying extents of fractional crystallization from such least-evolved granitoid samples can explain the entire data range (e.g., SiO_2/MgO) of the Laoshan granite (see below). We emphasize the above modeling and analysis to be conceptually significant for the petrogenesis of the magmas parental to the Laoshan granite. We also emphasize the estimated relative contributions of both crust and lithospheric mantle to be meaningful, although the exact mass contributions cannot be well constrained because of the many uncertainties discussed above.

ACCEPTED MANUSCRIPT

5.3 Effect of crystallization on the petrogenesis of the Laoshan granite

The large compositional variation of the Laoshan granite in terms of SiO_2/MgO and the correlated variations with the abundances and ratios (i.e., A/NK and A/CNK) of other major elements result from varying extents of fractional crystallization from magmas parental to the Laoshan granite (Fig.5). With cooling and crystallization, SiO_2/MgO decreases and the correlated trends with Al_2O_3, CaO, K_2O Na_2O, $^{T}Fe_2O_3$, TiO_2 and P_2O_5 result from varying extent of fractional crystallization of alkali feldspar, plagioclase, amphibolite, biotite, sphene, ilmenite, apatite and zircon, which is consistent with the petrography. The crystallization of plagioclase and alkali-feldspar results in Sr depletion and the resulting high Rb/Sr, hence the variably high $^{87}Sr/^{86}Sr$ (Fig.7b; Shao et al., 2015) with ^{87}Sr largely resulting from radioactive decay of ^{87}Rb, hence, the significant $^{87}Sr/^{86}Sr$-$^{87}Rb/^{86}Sr$ bulk-rock isochron (Fig. 7b; Cavazzini, 1994; Mahood and Halliday, 1988; Sallet et al., 2000; Shao et al., 2105). Fig.10a shows that plagioclase and potassium feldspar fractionation is critical in controlling Rb and Sr abundances. Fig. 6 shows that potassium feldspar and plagioclase fractionation is the primary cause of the Sr depletion as manifested by the data trend in Sr-Rb space (Fig. 10a) and Sr-Ba space (Fig. 10b). The effect of plagioclase fraction is also obvious as shown by the Eu/Eu*-Sr/Sr* correlation (R^2=0.6801; Fig. 7a; Niu and O'Hara, 2009, Shao et al., 2015).

To explain four samples with lower middle REEs from Sm to Tm (Fig. 6), we tried different mineral assemblages based on the petrography in fractional crystallization modeling (Fig.10c). The parental magma composition is assumed to be the value of QD15-01, which is not that highly evolved. Calculations indicate that the REE pattern is mainly controlled by fractionation of

ACCEPTED MANUSCRIPT

amphibole, apatite and plagioclase. By assuming co-precipitation modes of 42% amphibole, 0.03% apatite and 57.97% plagioclase, about 50% to 60% fractional crystallization of these minerals can form REE patterns similar to those of the four samples (Fig. 10c).

In summary, the primary magma parental to the Laoshan granite was derived by partial melting of the lower crust induced by and mixed with basaltic melts derived from the lithospheric mantle. Varying extents of fractional crystallization of such parental magmas led to the variably evolved compositions of the Laoshan granite samples.

5.4 Tectonic significance

As discussed above, the magma parental to the Laoshan granite was derived from lower continental crustal melting induced by lithospheric mantle-derived basaltic melts in an intraplate setting. The origin of the basaltic melts has been interpreted as relating to the Mesozoic subcontinental lithosphere thinning in eastern continental China (Fan et al., 2001; Gao et al., 2002; Guo et al., 2014; Liang et al., 2017; Liu et al., 2008; Niu, 2005; Niu et al., 2015). What is the mechanism of the lithospheric thinning and the cause of extensive granitoid magmatism in the Jurassic-Cretaceous Mesozoic? (1) Mantle plumes have been proposed as a mechanism causing the Mesozoic lithosphere thinning and the intra-plate magmatism in eastern China (Deng et al., 2004), but contemporary continental flood basalts with domal uplift expected to be associated with mantle plumes (He et al., 2003) are missing in eastern China. Besides, the observation that the "cold" subducted Paleo- Pacific slab lies in the mantle transition-zone (between 410 and 660 km seismic discontinuities) beneath eastern China (Zhao, 2009) argues against the presence and working of hot mantle plumes beneath eastern China (Niu, 2005). (2) Lithosphere delamination

ACCEPTED MANUSCRIPT

(e.g., Gao et al., 2009; Xu et al., 2006) is unlikely to happen because the compositionally buoyant subcontinental lithosphere cannot sink into the compositionally dense asthenosphere (Niu, 2005). (3) Lithosphere stretching induced asthenosphere upwelling can be ruled out because there is no stretching-related linear magmatism in eastern continental China (Niu, 2005).

Physically, the most likely mechanism is the basal hydration weakening by converting the basal portions of the lithosphere (i.e., subcontinental lithospheric mantle or SCLM into the asthenosphere accompanied by partial melting and basaltic magmatism (Niu, 2005, 2006, 2009, 2014; Niu et al., 2015). That is, the paleo-Pacific plate lying stagnant in the mantle transition zone release water by dehydration (Niu,2005). The water ascent in the form of hydrous melt can effectively hydrate the basal portion of the lithosphere and convert it to rigidity, strength and viscosity highly reduced asthenosphere (Niu, 2005, 2014), hence the lithosphere being thinned. Niu et al. (2015) demonstrate that the random distribution of the Jurassic-Cretaceous (~190 to ~90 Ma) granitoids in eastern continental China in space and time is best explained as a special consequence of plate tectonics. They were genetically associated with the paleo-Pacific plate lying stagnant in the mantle transition zone beneath eastern continental China (Niu, 2005, 2014; Niu et al., 2015). Underplating and intrusion of the basaltic magmas as the result of lithospheric mantle melting caused by basal hydration weakening indirectly caused the crustal melting and the widespread granitoid magmatism in the interiors of eastern continental China (Niu et al., 2015). In summary, the origin of the Laoshan granite is consistent with the origin of the Cretaceous granitoids in the continental interiors of eastern China as discussed in Niu et al. (2015). It is genetically associated with the lithosphere thinning by means of basal hydration weakening (Niu,

ACCEPTED MANUSCRIPT

2005, 2014) with the water ultimately, in the form of hydrous melt, coming from dehydration of the paleo-Pacific plate lying stagnant in the mantle transition zone (see Fig. 11; Niu et al., 2015).

Xue et al. (2018) proposed that the petrogenesis of the Cretaceous granitoids along the southeast coast of continental China is more directly related to the active subduction of the paleo-Pacific plate with the mantle wedge derived basaltic melts (the more depleted endmember) intruding/underplating the overlying crust. Figs. 8 and 9 show that the Laoshan granite differs distinctly from those of the coastal granitoids (Xue et al., 2018; Hong et al., 2018). The result of the comparison is mutually corroborating with our understanding that the Laoshan granite was formed in the intraplate setting, rather than an active subduction setting. This observation supports the hypothesis of Niu et al. (2015) that the Cretaceous granitoids in the continental interiors of eastern China is a consequence of the lithosphere thinning by means of basal hydration weakening. The magmatism of the granitoids is ultimately controlled by the dehydration of the paleo-Pacific plate lying stagnant in the mantle transition zone (Niu, 2005, 2014).

Conclusions

1. The primary magmas parental to the Laoshan granite were derived by anatexis of the lower continental crust heated by and mixed with lithosphere-derived basaltic melts.

2. The large compositional variation of the Laoshan granite results from varying extent of fractional crystallization as expressed in the SiO_2/MgO variation diagrams.

3. The Laoshan granite, like other widespread Cretaceous granitoids in the continental interiors of eastern China, is genetically associated with the lithosphere thinning by means of basal hydration

ACCEPTED MANUSCRIPT

weakening (Niu et al., 2005). The magmatism is ultimately controlled by dehydration of the paleo-Pacific plate lying stagnant in the mantle transition zone, which releases water in the form of hydrous melt. The melts ascend and convert the basal portions of the mantle lithosphere into the viscosity-reduced asthenosphere.

Acknowledgements

This work was supported by the grants from Qingdao National Laboratory for Marine Science and Technology (2015ASKJ03), NSFC-Shandong Joint Fund for Marine Science Research Centers (U1606401), National Natural Science Foundation of China (41130314, 41630968), the Chinese Academy of Sciences Innovation (Y42217101L) and the 111 Project (B18048). We thank Jiyong Li, Guodong Wang, Juanjuan Kong, Fengli Shao, Di Hong for the field work. We thank reviewers for useful comments.

ACCEPTED MANUSCRIPT

ACCEPTED MANUSCRIPT

References

Bacon, C.R., Druitt, T.H., 1988. Compositional Evolution of the Zoned Calcalkaline Magma Chamber of Mount-Mazama, Crater Lake, Oregon. Contributions to Mineralogy and Petrology 98, 224-256.

Bergantz, G. W., 1989. Underplating and partial melting: implications for melt generation and extraction. Science 254, 1039-1095.

Cai, Y.C., Fan, H.R., Santosh, M., Hu, F.F., Yang, K.F., Hu, Z., 2015. Subduction-related metasomatism of the lithospheric mantle beneath the southeastern north china craton: Evidence from mafic to intermediate dykes in the northern Sulu orogeny. Tectonophysics 659, 137–151.

Cavazzini, G., 1994. Increase of $^{87}Sr/^{86}Sr$ in residual liquids of high-Rb/Sr magmas that evolve by fractional crystallization. Chemical Geology 118, 321-326.

Chappell, B.W., White, A.J.R., 2001. Two contrasting granite types: 25 years later. Australian Journal of Earth Sciences 48, 489-499.

Chen, S., Wang, X.H., Niu, Y.L., Sun, P., Duan, M., Xiao, Y.Y., Guo, P.Y., Gong, H.M., Wang, G.D., Xue, Q.Q., 2017. Simple and cost-effective methods for precise analysis of trace element abundances in geological materials with ICP-MS. Science Bulletin 62, 277-289.

Cox, K.G., Bell, J.D., Pankhurst, R.J., 1979. The interpretation of igneous rocks, George Allen and Unwin, London.

Deng, J.F., Mo, X.X., Zhao, H.L., Wu, Z.X., Luo, Z.H., Su, S.G., 2004. A new model for the dynamic evolution of Chinese lithosphere: 'continental roots–plume tectonics'. Earth Science Reviews 65, 223–275.

Ewart, A., Griffin, W.L., 1994. Application of Proton-Microprobe Data to Trace-Element Partitioning in Volcanic-Rocks. Chemical Geology 117, 251-284.

ACCEPTED MANUSCRIPT

Fan, W. M., Guo, F., Wang, Y. J., Lin, G., Zhang, M., 2001. Post-orogenic bimodal volcanism along the Sulu orogenic belt in eastern China. Physics and Chemistry of the Earth, Part A: Solid Earth and Geodesy 26, 733-746.

Gao, S., Luo, T. C., Zhang, B. R., Zhang, H. F., Han, Y. W., Zhao, Z. D., Hu, Y. K., 1998. Chemical composition of the continental crust as revealed by studies in East China. Geochimica et Cosmochimica Acta 62, 1959-1975.

Gao, S., Rudnick, R. L., Carlson, R. W., Mcdonough, W. F., Liu, Y. S., 2002. Re–os evidence for replacement of ancient mantle lithosphere beneath the north china craton. Earth and Planetary Science Letters 198, 307-322.

Gao, S., Zhang, J.F., Xu, W.L., Liu, Y.S., 2009. Delamination and destruction of the North China Craton. Chinese Science Bulletin 54, 3367–3378.

Goss, S.C., Wilde, S.A., Wu, F.Y., Yang, J.H., 2010. The age, isotopic signature and significance of the youngest Mesozoic granitoids in the Jiaodong Terrane, Shandong Province, North China Craton. Lithos 120, 309-326.

Ghiorso, M. S., Sack, R. O., 1995. Chemical mass transfer in magmatic processes IV. A revised and internally consistent thermodynamic model for the interpolation and extrapolation of liquid-solid equilibria in magmatic systems at elevated temperatures and pressures. Contributions to Mineralogy and Petrology 119, 197-212.

Guo, J.H., Chen, F.K., Zhang, X.M., Siebei, W., Zhai, M.G., 2005. Evolution of syn- to post-collisional magmatism from north Sulu UHP belt, eastern China: Zircon U-Pb geochronology. Acta Petrologica Sinica 21, 1281-1301 (in Chinese with English abstract).

Guo, J., Guo, F., Wang, C. Y., Li, C., 2013. Crustal recycling processes in generating the early Cretaceous Fangcheng basalts, North China Craton: New constraints from mineral chemistry, oxygen isotopes of olivine and whole-rock geochemistry. Lithos 170, 1-16.

ACCEPTED MANUSCRIPT

Guo, P.Y., Niu, Y.L., Ye, L., Liu, J.J., Sun, P., Cui, H.X., Zhang, Y., Gao, J.P., Su, L., Zhao, J.X., Feng, Y.X., 2014. Lithosphere thinning beneath west North China Craton: evidence from geochemical and Sr-Nd-Hf isotope compositionsof Jining basalts. Lithos 202, 37-54.

Halliday, A.N., Davidson, J.P., Hildreth, W., Holden, P., 1991. Modelling the petrogenesis of high Rb/Sr silicic magmas. Chemical Geology 92, 107-114.

Hart, S.R., 1984. A large-scale isotope anomaly in the southern Hemisphere mantle. Nature 309, 753–757.

He, B., Xu, Y.G., Chung, S.L., Xiao, L., Wang, Y., 2003, Sedimentary evidence for a rapid crustal doming prior to the eruption of the Emeishan flood basalts: Earth and Planetary Science Letters 213, 389–403.

Hong, D., Niu, Y.L., Xiao, Y.Y., Sun, P., Kong, J.J., Guo, P.Y., Shao, F.L., Wang, X.H., Duan, M., Xue, Q.Q., Gong, H.M., Chen, S., 2018. Origin of the Jurassic-Cretaceous intraplate granitoids in Eastern China as a consequence of paleo-Pacific plate subduction. Lithos 322, 405-419.

Huppert H.E., Sparks, R.S.J., 1988. The generation of granitic magmas by intrusion of basalt into continental crust. Journal of Petrology 29, 599–624.

Hu, B., Zhai, M., Li, T., Li, Z., Peng, P., Guo, J., Kusky, T. M., 2012. Mesoproterozoic magmatic events in the eastern North China Craton and their tectonic implications: Geochronological evidence from detrital zircons in the Shandong Peninsula and North Korea. Gondwana Research 22, 828-842.

Jahn, B.M., Wu, F.Y., Lo, C.H., Tsai, C.H., 1999. Crust-mantle interaction induced by deep subduction of the continental crust: geochemical and Sr-Nd isotopic evidence from post-collisional mafic–ultramafic intrusions of the northern Dabie complex, central China. Chemical Geology 157, 119-146.

Jahn, B. M., Liu, D., Wan, Y., Song, B., Wu, J. 2008. Archean crustal evolution of the Jiaodong Peninsula, China, as revealed by zircon SHRIMP geochronology, elemental and Nd-isotope geochemistry. American Journal of Science 308, 232-269.

ACCEPTED MANUSCRIPT

King, P.L., White, A.J.R., Chappell, B.W., Allen, C.M., 1997. Characterization and origin of aluminous A-type granites from the Lachlan Fold Belt, southeastern Australia. Journal of petrology 38, 371-391.

Li, H., Ling M.X., Ding, X., Zhang, H., Li, C.Y., Liu D.Y., Sun, W.D., 2014. The geochemical characteristics of Haiyang A-type granite complex in Shandong, eastern China. Lithos 200, 142-156.

Liang, Y., Liu, X., Qin, C., Li, Y., Chen, J., Jiang, J.Y., 2017. Petrogenesis of Early Cretaceous mafic dikes in southeastern Jiaolai basin, Jiaodong Peninsula, China. International Geology Review 59, 131-150.

Liu, S., Hu, R., Gao, S., Feng, C.X., Qi, Y.Q., Wang, T., Feng, G.Y., Coulson, I.M., 2008. U-Pb zircon age, geochemical and Sr-Nd-Pb-Hf isotopic constraints on age and origin of alkaline intrusions and associated mafic dikes from Sulu orogenic belt, Eastern China. Lithos 106, 365-379

Liu, Y.S., Hu, Z.C., Zong, K.Q., Gao, C.G., Gao, S., Xu, J., Chen, H.H., 2010. Reappraisement and refinement of zircon U-Pb isotope and trace element analyses by LA-ICP-MS. Chinese Science Bulletin 55, 1535-1546.

Ludwig, K.R., 2003. User's Manual for Isoplot 3.0: a Geochronological Toolkit for Microsoft Excel, Berkeley Geochronology Center, Berkeley.

Ma, L., Jiang, S.Y., Hofmann, A.W., Dai, B.Z., Hou, M.L., Chen, L.H., Jiang, Y.H., 2014. Lithospheric and asthenospheric sources of lamprophyres in the Jiaodong Peninsula: a consequence of rapid lithospheric thinning beneath the North China Craton? Geochimica et cosmochimica Acta 124, 250-271.

Ma, L., Jiang, S. Y., Hofmann, A. W., Xu, Y. G., Dai, B. Z., Hou, M. L., 2016. Rapid lithospheric thinning of the north china craton: new evidence from cretaceous mafic dikes in the jiaodong peninsula. Chemical Geology 432, 1-15.

Mahood, G. A., Halliday, A. N., 1988. Generation of high-silica rhyolite: a Nd, Sr, and O isotopic study of Sierra La Primavera, Mexican Neovolcanic Belt. Contributions to Mineralogy and Petrology 100, 183-191.

ACCEPTED MANUSCRIPT

Maitre L., Bateman R.W., Dudek, P., Keller, A., Lameyre, J., Bas, J.L., Sabine M.J., Schmid, P.A., Sorensen, S., Streckeisen, H., Woolley, A., Zanettin, A.R., 1989. A classification of igneous rocks and glossary of terms: Recommendations of the International Union of Geological Sciences, Subcommission on the Systematics of Igneous Rocks, 193.

Míková, J., Denková, P., 2007. Modified chromatographic separation scheme for Sr and Nd isotope analysis in geological silicate samples. Journal of Geosciences 52, 221-226.

Nash, W.P., Crecraft, H.R., 1985. Partition coefficients for trace elements in silicic magmas. Geochimica et Cosmochimica Acta 49, 2309-2322.

Niu, Y.L., 2005. Generation and evolution of basaltic magmas: some basic concepts and a hypothesis for the origin of the Mesozoic–Cenozoic volcanism in eastern China. Geological Journal of China Universities 11, 9-46.

Niu, Y.L., 2014. Geological understanding of plate tectonics: Basic concepts, illustrations, examples and new perspectives. Global Tectonics and Metallogeny 10, 23-46.

Niu, Y.L., O'Hara, M.J., 2009. MORB mantle hosts the missing Eu (Sr, Nb, Ta and Ti) in the continental crust: New perspectives on crustal growth, crust–mantle differentiation and chemical structure of oceanic upper mantle. Lithos 112, 1-17.

Niu, Y.L., Liu, Y., Xue, Q.Q., Shao F.L., Chen, S., Duan, M., Guo, P.Y., Gong, H.M., Hu, Y., Hu Z.X., Kong, J.J., 2015. The exotic origin of the continental shelf of East and South China Seas—a testable hypothesis with consequences on the tectonic evolution of the western Pacific and eastern China since the Mesozoic. Science Bulletin 18, 1598-1616.

Niu, Y.L., Tang, J., 2016. Origin of the Yellow Sea: An insight. Science Bulletin 61, 1076-1080.

Oh, C.W., Kusky, T., 2007. The late Permian to Triassic Hongseong-Odesan Collision Belt in South Korea, and its tectonic correlation with China and Japan. Int Geol Rev 49, 636–657.

ACCEPTED MANUSCRIPT

Patiño Douce, A. E., 1997. Generation of metaluminous A-type granites by low-pressure melting of calc-alkaline granitoids. Geology 25, 743-746.

Qiu, J.S., Xiao, E., Hu, J., Xu, X.S., Jiang, S.Y., Li, Z., 2008. Petrogenesis of highly fractionated Itype granites in the coastal area of northeastern Fujian Province: constraints from zircon U-Pb geochronology, geochemistry and Nd-Hf isotopes. Acta Petrologica Sinica 24, 2468-2484 (in Chinese with English abstract).

Sallet, R., Moritz, R., Fontignie, D., 2000. Fluorite $^{87}Sr/^{86}Sr$ and REE constraints on fluid–melt relations, crystallization time span and bulk D_{Sr} of evolved high-silica granites. Tabuleiro granites, Santa Catarina, Brazil. Chemical Geology, 164, 81-92.

Shao, F.L., Niu, Y.L., Regelous, R., Zhu, D.C., 2015. Petrogenesis of peralkaline rhyolites in an intra-plate setting: Glass House Mountains, Southeast Queensland, Australia. Lithos 216/217, 196-210.

Skjerlie, K. P., Johnston, A. D., 1992. Vapor-absent melting at 10 kbar of a biotite- and amphibole-bearing tonalitic gneiss: implications for the generation of a-type granites. Geology 20, 263-266.

Sun, S.S., McDonough, W., 1989. Chemical and isotopic systematics of oceanic basalts: implications for mantle composition and processes. Geological Society, London, Special Publications 42, 313-345.

Sun, P., Niu, Y.L., Guo, P.Y., Ye, L., Liu, J.J., Feng, Y.X., 2017. Elemental and Sr-Nd-Pb isotope geochemistry of the Cenozoic basalts in Southeast China: Insights into their mantle sources and melting processes. Lithos 272-273, 16-30.

Tang, J., Xu, W.L., Niu, Y.L., Wang, F., Ge, W.C., Sorokin, A.A., Chekryzhov, I.Y., 2016. Geochronology and geochemistry of Late Cretaceous–Paleocene granitoids in the Sikhote-Alin Orogenic Belt: Petrogenesis and implications for the oblique. Lithos 266-267, 202-212.

Vervoort, J. D., Patchett, P. J., 1996. Behavior of hafnium and neodymium isotopes in the crust: constraints from precambrian crustally derived granites. Geochimica Et Cosmochimica Acta 60, 3717-3733.

ACCEPTED MANUSCRIPT

Wang, D.Z., Zhao, G.T., Qiu, J.S., 1995. The tectonic constraint on the late mesozoic A-type granitoids in Eastern China. Geological Journal of Universities 2, 13-21 (in Chinese with English abstract).

Wang, R. C., Wang, D. Z., Zhao, G. T., Lu, J. J., Chen, X. M., Xu, S. J., 2001. Accessory mineral record of magma-fluid interaction in the laoshan I- and A-type granitic complex, eastern china. Physics and Chemistry of the Earth, Part A: Solid Earth and Geodesy 26, 835-849.

Wei, C. S., 2008. ^{207}Pb–^{208}Pb decoupling of alkali feldspar from a late Mesozoic A-type granite in eastern China. Mineralogy and Petrology 94, 209.

Whalen, J.B., Currie, K.L., Chappell, B.W., 1987. A-type granites: geochemical characteristics, discrimination and petrogenesis. Contributions to mineralogy and petrology 95, 407-419.

Wiedenbeckliu, M., Allé, P., Corfu, F., Griffin, W.L., Meier, M., Oberli, F., Quadt, A.V., Roddick, J.C., Spiegel, W., 1995. Three Natural Zircon Standards for U-Th-Pb, Lu-Hf, Trace element and REE Analyses. Geostandards and Geoanalytical Research 19, 1-23.

Wilson, M., 1989. Igneous Petrogenesis, Unwin Hyman, London.

Wu, F.Y., Sun, D.Y., Li, H.M., Jahn, B.M., Wilde, S., 2002. A-type granites in northeastern China: age and geochemical constraints on their petrogenesis. Chemical Geology 187, 143-173.

Xue, Q.Q., Niu, Y.L., Chen, S., Sun, P., Duan, M., Gao, Y.J., Hong, D., Xiao, Y.Y., Wang, X.H., Guo, P.Y., 2018. Tectonic significance of Cretaceous granitoids along the southeast coast of continental China. Geological Journal, 1-24.

Xu, W.L., Wang, Q.H., Wang, D.Y., Guo, J.H., Pei, F.P., 2006. Mesozoic adakitic rocks from the Xuzhou–Suzhou area, eastern China: evidence for partial melting of delaminated lower continental crust. Journal of Asian Earth Sciences 27, 454–464.

ACCEPTED MANUSCRIPT

Yan, Q.S., Shi, X.F., 2014. Geochemistry and petrogenesis of the Cretaceous A‐type granites in the Laoshan granitic complex, eastern China. Island Arc 23, 221-235.

Yang, J.H., Chung, S.L., Wilde, S.A., Wu, F.Y., Chu, M.F., Lo, C.H., Fan, H.R., 2005a. Petrogenesis of post-orogenic syenites in the Sulu Orogenic Belt, East China: geochronological, geochemical and Nd–Sr isotopic evidence. Chemical Geology 214, 99-125.

Yang, J.H., Wu, F.Y., Chung S.L., Wilde, S.A., Chu, M.F., Lo, C.H., Song, B., 2005b. Petrogenesis of Early Cretaceous intrusions in the Sulu ultrahigh-pressure orogenic belt, east China and their relationship to lithospheric thinning. Chemical Geology 222, 200-231.

Yang, Y.H., Zhang, H.F., Chu, Z.Y., Xie, L.W., Wu, F.Y., 2010. Combined chemical separation of Lu, Hf, Rb, Sr, Sm and Nd from a single rock digest and precise and accurate isotope determinations of Lu-Hf, Rb-Sr and Sm-Nd isotope systems using Multi-Collector ICP-MS and TIMS. International Journal of Mass Spectrometry 290, 120-126.

Ying, J., Zhang, H., Kita, N., Morishita, Y., Shimoda, G., 2006. Nature and evolution of Late Cretaceous lithospheric mantle beneath the eastern North China Craton: Constraints from petrology and geochemistry of peridotitic xenoliths from Jünan, Shandong Province, China. Earth and Planetary Science Letters 244, 622-638.

Zhai, M.G., Guo, J.H., Liu, W.J., 2005. Neoarchean to paleoproterozoic continental evolution and tectonic history of the North China Craton: a review. J Asian Earth Sci 24, 547–561.

Zhai, M.G., Guo, J.H., Li, Z., Hou, Q.L., Peng, P., Fan, Q.C., Li, T.S., 2007. Linking Sulu orogenic belt to Korean Peninsula: evidences of metamorphism, Precambrian basement and Paleozoic basins. Gondwana Research 12, 388–403.

ACCEPTED MANUSCRIPT

Zhai, M. G., Zhang, Y. B., Zhang, X. H., Wu, F. Y., Peng, P., Li, Q. L., Hou, Q.L., Li, T.S., Zhao, L., 2016. Renewed profile of the mesozoic magmatism in korean peninsula: regional correlation and broader implication for cratonic destruction in the north china craton. Science China Earth Sciences 59, 1-34.

Zhang, J., Zhang, H., Kita, N., Shimoda, G., Morishita, Y., Ying, J., Tang, Y., 2011. Secular evolution of the lithospheric mantle beneath the eastern North China craton: evidence from peridotitic xenoliths from Late Cretaceous mafic rocks in the Jiaodong region, east-central China. International Geology Review 53, 182-211.

Zhang, H.F., Sun, Y.L., Tang, Y.J., Xiao, Y., Zhang, W.H., Zhao, X.Z., Santosh, M., Menzies, M.A., 2012. Melt-peridotite interaction in the Pre-Cambrian mantle beneath the western North China Craton: Petrology, geochemistry and Sr, Nd and Re isotopes. Lithos 149, 100-114.

Zhao, D.P., 2009. Multiscale seismic tomography and mantle dynamics. Gondwana Research 15, 297–323.

Zhao, G.T., Wang, D.Z., Cao, Q.C., 1997. The geochemistry and genesis of the Laoshan Granitoids, Shandong Province. Geological Journal of China Universities 3, 1-15 (in Chinese with English abstract).

Zhao, X.X., Coe, R.S., Chang, K.H., Park, S., Omarzai, S.K., Zhu, R.X., Zhou, Y.X., Gilder, S., Zheng, Z., 1999. Clockwise rotations recorded in Early Cretaceous rocks of South Korea: implications for tectonic affinity between the Korean Peninsula and North China. Geophys J Int 139,447–463.

Zhao, Z.F., Zheng, Y.F., Chen, Y.X., Sun, G.C., 2017. Partial melting of subducted continental crust: Geochemical evidence from synexhumation granite in the Sulu orogen. Geological Society of America Bulletin 129, 1692-1707.

Zhou, X.M., Li, W.X., 2000. Origin of Late Mesozoic igneous rocks of southeastern China: implications for lithosphere subduction and underplating of mafic magma. Tectonophysics 326, 269–287.

ACCEPTED MANUSCRIPT

Zhou, X., Sun, M., Zhang, G., Chen, S., 2002. Continental crust and lithospheric mantle interaction beneath North China: isotopic evidence from granulite xenoliths in Hannuoba, Sino-Korean craton. Lithos 62, 111-124.

Zhou, X.M., Sun, T., Shen, W.Z., Shu, L.S., Niu, Y.L., 2006. Petrogenesis of Mesozoic granitoids and volcanic rocks in South China: a response to tectonic evolution. Episodes 29, 26–33.

Zindler, A., Hart, S., 1986. Chemical geodynamics. Annual review of earth and planetary sciences 14, 493-571.

ACCEPTED MANUSCRIPT

ACCEPTED MANUSCRIPT

Figure captions

Fig. 1 (a) Simplified geological framework of eastern continental China. (b) Distribution of the Mesozoic intrusive and eruptive rocks in the Jiaodong Peninsula and the locations of the Laoshan granite and nearby intrusions (modified after the geological map of Shandong Province in 1/1,500,000 scale from the Geological Atlas of China). (c) Geological sketch of the Laoshan granite and sample locations (modified after the Laoshan geological map of 1/200,000 scale).

Fig. 2 Photograph in the field and photomicrographs in cross-polarized light. (A) shows the sharp contact of mafic magmatic enclave with the host granite (QD15-03); (B) shows the mineral assemblage and the granophyric texture of alkali feldspar granite (LS15-15); (C) shows the mineral assemblage of monzonitic granite (LS15-21); (D) shows fluorite in QD15-04. Afs = alkali feldspar; Pl = plagioclase; Qtz = quartz; Am = amphibole; Bi = biotite; Ap = apatite; Sph = sphene; Fl = Flourite.

Fig.3 The Concordia diagrams show zircon U-Pb ages and representative CL images of zircons with analytical spots as indicated with yellow circles for LS15-15 and QD15-22. See Table 2 for analytical data.

Fig.4 Portion of the total alkali versus silica (TAS) diagram (Cox et al., 1979; Wilson, 1989; Maitre et al., 1989) shows the compositional variation of samples. The curved solid line subdivides the alkalic (above) from sub-alkalic (below) rock types (Wilson, 1989; Maitre et al., 1989). The A-type granite and I-type granite are literature data of Laoshan granitoid rocks (Zhao et al., 1997; Yan and Shi, 2014).

ACCEPTED MANUSCRIPT

Fig.5 Bivariate plots of the major element oxides and ratios (e.g., A/NK= molar Al_2O_3 /[Na_2O+K_2O], A/CNK = molar Al_2O_3 /[CaO+Na_2O+K_2O]) as a function of SiO_2/MgO show a large range of major element compositional variation, reflecting a varying degree of fractional crystallization of plagioclase, alkali feldspar, amphibole, biotite and accessory phases as observed. The A-type granite and I-type granite are the literature data as Fig.4.

Fig.6 Chondrite-normalized rare earth element and primitive mantle normalized incompatible element patterns for the Laoshan granite. For comparison, the literature data (A-type granite, I-type granite; see Fig.4) are also plotted. Chondrite and primitive mantle values are from Sun and McDonough (1989). Samples show various Eu anomalies as the result of plagioclase and alkali feldspar fractionation as Fig.7a. The lower values of middle rare earth elements from Sm to Tm in the four samples is mainly controlled by fractionation of amphibole, apatite and plagioclase.

Fig.7 (a) The correlation between Eu/Eu* and Sr/Sr* (R^2=0.7593; Fig. 7a) indicates the consequence of plagioclase-dominated fraction (Niu and O'Hara, 2009, Shao et al., 2016). (b) Rb/Sr isochron defined by Laoshan granite samples give a significant and consistent emplacement age of ~ 126 Ma, which is, expectedly, slightly older than the zircon crystallization ages (Fig. 3). Importantly, the isochron gives a tight and significant initial $^{87}Sr/^{86}Sr$ of 0.7061, pointing to uniform source (or mixed source) composition for the Laoshan granite.

Fig.8 Hf-Nd isotope diagram illustrates that magmas parental to the Laoshan granite are derived from anatexis of the lower continental crust induced by and mixed with lithospheric mantle-derived basaltic magmas beneath eastern continental China. Binary isotope mixing calculations with the number of basaltic melts contribution use the lithosphere mantle-derived

ACCEPTED MANUSCRIPT

melts data from Guo et al. (2013) and Liang et al. (2017) and the lower continental crust (LCC) data from Jahn et al (2008), in 5% intervals. Hf isotope of the literature data is inferred from Nd isotope following the equation (ε_{Hf}=1.36ε_{Nd}+2.95) given by Vervoort and Patchett (1996). The coastal granitiods are from Xue et al. (2018).

Fig.9 (a) Initial $^{207}Pb/^{204}Pb$ vs. initial $^{206}Pb/^{204}Pb$ and (b) initial $^{206}Pb/^{204}Pb$ vs. initial $^{208}Pb/^{204}Pb$ diagrams show the Laoshan granites differ distinctly from those of the coastal granitoids (Hong et al., 2018). The North Hemisphere Reference Line (NHRL) refers to what from Hart (1984). EM2 fields after Zindler and Hart (1986) are also shown.

Fig.10 (a), (b) Rb-Sr and Ba-Sr covariation diagram, indicating that the evolution of the Laoshan granite was controlled largely by alkali-feldspar fractionation. Mineral fractionation vectors (Kf = K-feldspar; Pl = plagioclase; Am = amphibole; Bi=biotite) calculated using partition coefficients from Ewart and Griffin (1994), Nash and Crecraft (1985) and Bacon and Druitt (1988). Tick marks indicate the percentage of mineral phase removed, in 10% intervals. See Appendix 4 for relevant partition coefficients used to calculate. (c) Shows 20%, 30%, 50%, 60% fractional crystallization of the mineral assemblages of Model from assumed magma (QD15-01) along with the Laoshan granite on chondrite normalized rare earth element diagram. (d) Fe_2O_3 vs. SiO_2/MgO. The MELTS (Ghiorso and Sack, 1995) used for the modeling is set at 10 kbars with the temperature range of 1200-700°C at 20K intervals. The composition of 90DA1-Granulite (Zhou et al. 2002) and YC-LCC (Gao et al., 1998) represent source materials of the partial melting modelling. Tick marks indicate the composition of melts, and the numbers show the extent of partial melting. The details of the calculation result and the mineral composition of the residues

ACCEPTED MANUSCRIPT

are compiled in Appendix 5. The composition of mixing magma is calculated by using data of the melts of granulite (90%) with the partial melting range of 7% - 28% and the data of dolerite (LYYJ2-1) from Liang et al. (2017) represented the mantle-derived basaltic contribution (10%).

Fig. 11 The conceptual model of the Cretaceous magmatism in the NW-SE cross section (modified after Niu et al., 2015) shows the intra-plate tectonic setting and origin of magmas parental to the Laoshan granite. The stagnant paleo-Pacific slab in the Mesozoic released water in the form of hydrous melts that ascended and weakened and converted the basal portions of the mantle lithosphere into asthenosphere while producing basaltic magma from the being-converted mantle lithosphere. Such magma rose and intruded the continental crust, providing both heat and material for the parental magmas of the Laoshan granite.

Table caption

Table 1 Petrography of the samples from the Laoshan granite (N=27).

Table 1 Petrography of the samples from the Laoshan granite (N=27).

Sample	Rock Type	GPS		Mineral composition (%)			
		Latitude (N)	Longitude (E)	Pl	A	Q	Others
LS15-06	alkali-feldspar granite	36.13	120.57	2	56	40	Mt, Bi, Ap
LS15-07	alkali-feldspar granite	36.15	120.52	4	58	35	Amp, Bi, Mt, Zrn
LS15-08	syenogranite	36.18	120.50	12	45	38	Amp, Bi, Mt
LS15-11	alkali-feldspar granite	36.20	120.55	6	54	34	Amp, Bi, Mt, Zrn, Ap
LS15-15	alkali-feldspar granite	36.25	120.62	3	64	28	Amp, Mt, Sph, Zrn
LS15-16	alkali-feldspar granite	36.27	120.60	3	62	30	Bi, Mt, Sph
LS15-19	alkali-feldspar granite	36.24	120.56	5	55	36	Mt, Amp, Bi, Chl
LS15-20	alkali-feldspar granite	36.24	120.57	4	53	40	Bi, Mt, Amp
LS15-21	syenogranite	36.09	120.42	20	43	30	Amp, Bi, Mt, Sph, Zrn, Ap
LS15-23	syenogranite	36.19	120.46	20	38	35	Bi, Ap, Mt, Zrn, Amp
LS15-25	syenogranite	36.19	120.43	30	40	25	Bi ,Amp, Ap, Mt, Zrn,Sph

ACCEPTED MANUSCRIPT

LS15-28	alkali-feldspar granite	36.11	120.37	3	44	48	Mt
LS15-30	alkali-feldspar granite	36.07	120.36	5	46	45	Bi, Mt, Zrn
QD15-01	syenogranite	36.39	120.87	15	47	30	Amp, Bi, Mt, Zrn, Sph
QD15-02	monzonitic granite	36.39	120.87	35	40	20	Amp, Bi, Mt, Zrn
QD15-03	monzonitic granite	36.41	120.87	35	38	22	Amp, Bi, Mt, Zrn
QD15-04	syenogranite	36.49	120.86	10	43	40	Bi, Ap, Mt, Zrn, Chl, Fl
QD15-08	alkali-feldspar granite	36.39	120.67	3	66	20	Bi, Mt, Chl
QD15-10	syenogranite	36.37	120.62	12	42	38	Bi, Ap, Mt, Zrn
QD15-11	alkali-feldspar granite	36.37	120.59	5	53	40	Bi, Ap, Mt, Zrn
QD15-14	syenogranite	36.32	120.58	20	35	40	Bi, Ap, Mt, Zrn
QD15-17	monzonitic granite	36.00	120.28	35	32	30	Bi, Mt
QD15-24	syenogranite	36.03	120.04	25	43	30	Bi, Mt, Ap
QD15-19	syenogranite	35.99	120.11	13	43	40	Bi, Amp, Mt
QD15-22	monzonitic granite	36.03	120.11	36	38	20	Bi, Amp, Mt, Sph
QD15-25	syenogranite	35.94	120.10	23	52	20	Amp, Bi, Mt, Chl
QD15-27	syenogranite	35.94	120.06	15	55	25	Bi, Ap, Mt, Zrn, Amp

Pl=Plagioclase; A=Alkali feldspar; Q=Quartz; Bi=Biotite, Amp=Amphibole, Ap=Apatite, Mt=Magnetitie, Zrn=Zircon, Fl=Fluorite, Sph=Sphene, Chl=Chlorite.

Table 2 LA-ICPMS zircon U-Pb data of Laoshan granites.

Table 2 LA-ICPMS zircon U-Pb data of Laoshan granites.

Spot	Content (ppm)				Ratios						Age (Ma)			
	Pb	Th	U	Th/U	$^{207}Pb/^{206}Pb$	1σ	$^{207}Pb/^{235}U$	1σ	$^{206}Pb/^{238}U$	1σ	$^{207}Pb/^{235}U$	1σ	$^{206}Pb/^{238}U$	1σ
QD15-22-1	7.42	301.55	224.15	1.35	0.0485	0.025	0.1222	0.063	0.0184	0.006	117.1	5.7	117.8	3.5
QD15-22-3	5.45	213.24	163.04	1.31	0.0469	0.027	0.1198	0.073	0.0186	0.006	114.9	6.6	118.8	3.6
QD15-22-4	9.85	438.03	260.53	1.68	0.0481	0.022	0.1223	0.062	0.0182	0.006	117.2	5.6	116.4	3.5
QD15-22-5	7.52	302.49	208.86	1.45	0.0506	0.029	0.1236	0.066	0.0184	0.006	118.4	6.0	117.5	4.0
QD15-22-6	7.13	275.54	200.57	1.37	0.0514	0.025	0.1257	0.057	0.0182	0.006	120.2	5.2	116.5	3.6
QD15-22=7	47.08	723.63	336.87	2.15	0.0479	0.017	0.1226	0.042	0.0187	0.003	117.4	3.8	119.3	1.9
QD15-22=8	6.74	105.83	48.56	2.18	0.0518	0.050	0.1255	0.0117	0.0188	0.005	120.1	10.5	120.2	3.3

ACCEPTED MANUSCRIPT

QD15-22=10	17.72	254.67	149.43	1.70	0.0491	0.024	0.1263	0.056	0.0190	0.004	120.8	5.1	121.1	2.3
QD15-22=13	20.01	287.18	219.96	1.31	0.0497	0.022	0.1252	0.058	0.0184	0.004	119.8	5.2	117.4	2.3
QD15-22=14	14.84	215.50	205.53	1.05	0.0471	0.024	0.1188	0.056	0.0187	0.003	114.0	5.0	119.3	2.2
QD15-22=15	15.67	215.90	175.35	1.23	0.0483	0.026	0.1255	0.061	0.0193	0.005	120.1	5.5	123.3	2.9
QD15-22=16	22.67	318.67	234.56	1.36	0.0487	0.019	0.1267	0.049	0.0191	0.003	121.1	4.4	121.8	2.1
QD15-22=17	27.88	421.41	251.20	1.68	0.0467	0.023	0.1156	0.051	0.0184	0.003	111.0	4.6	117.4	2.0
QD15-22=18	16.07	223.96	197.61	1.13	0.0513	0.026	0.1269	0.056	0.0185	0.004	121.3	5.0	118.4	2.3
QD15-22=20	20.91	322.50	174.28	1.85	0.0523	0.031	0.1302	0.070	0.0192	0.006	124.3	6.3	122.8	3.6
QD15-22=22	23.43	362.75	194.34	1.87	0.0529	0.024	0.1314	0.061	0.0193	0.007	125.4	5.5	123.3	4.4
LS15-15-3	9.49	403.35	290.85	1.39	0.0504	0.027	0.1278	0.072	0.0187	0.008	122.1	6.4	119.6	5.0
LS15-15-4	10.32	436.27	305.70	1.43	0.0487	0.023	0.1256	0.062	0.0192	0.008	120.1	5.6	122.3	4.9
LS15-15=7	14.24	185.48	197.24	0.94	0.0537	0.024	0.1362	0.060	0.0186	0.004	129.7	5.3	118.7	2.3
LS15-15=8	27.67	427.90	256.87	1.67	0.0529	0.025	0.1319	0.063	0.0182	0.003	125.8	5.6	116.5	1.8
LS15-15=10	12.12	168.76	140.59	1.20	0.0524	0.029	0.1319	0.068	0.0189	0.004	125.8	6.1	120.5	2.4
LS15-15=11	25.04	366.40	250.10	1.47	0.0512	0.022	0.1331	0.056	0.0191	0.004	126.9	5.1	122.2	2.7
LS15-15=12	35.49	485.57	294.23	1.65	0.0516	0.017	0.1375	0.047	0.0195	0.004	130.8	4.2	124.3	2.4
LS15-15=13	19.94	283.03	241.36	1.17	0.0483	0.024	0.1252	0.056	0.0191	0.004	119.8	5.1	122.2	2.4
LS15-15=14	43.81	655.64	439.44	1.49	0.0491	0.017	0.1251	0.044	0.0187	0.004	119.7	4.0	119.5	2.2
LS15-15=17	21.92	320.47	224.55	1.43	0.0495	0.026	0.1246	0.059	0.0190	0.005	119.2	5.3	121.6	3.2
LS15-15=18	16.42	242.23	195.54	1.24	0.0485	0.025	0.1256	0.071	0.0196	0.007	120.1	6.4	125.1	4.3
LS15-15=19	22.61	343.31	256.66	1.34	0.0517	0.026	0.1331	0.066	0.0200	0.007	126.9	5.9	127.4	4.4
LS15-15=20	16.05	214.84	206.54	1.04	0.0565	0.027	0.1514	0.072	0.0208	0.008	143.2	6.4	132.9	5.0

ACCEPTED MANUSCRIPT

LS15-15=21	16.64	225.52	182.64	1.23	0.0480	0.0026	0.1341	0.0069	0.0213	0.0007	127.8	6.1	135.9	4.5

Appendices

Appendix 1 Bulk-rock major elements of USGS reference materials run with samples.

Appendix 2 Bulk-rock trace elements of USGS reference materials run with samples.

Appendix 3 Bulk-rock Sr-Nd-Pb-Hf isotope of USGS reference materials JG-3 and BHVO-2 run with samples.

Appendix 4 Relevant partition coefficients.

Appendix 5 The calculation result of partial melting using MELTS.

Appendix 6 Bulk-rock major and trace elements compositions of Laoshan granites.

Appendix 7 Bulk-rock Sr-Nd-Pb-Hf isotopic compositions for Laoshan granites.

ACCEPTED MANUSCRIPT

ACCEPTED MANUSCRIPT

- The Laoshan granite resulted from fractional crystallization of the parental magma.
- Anatexis of the LCC heated by and mixed with basic magma formed the parental magma.
- The basal hydration weakening caused the lithosphere thinning with basic magmatism.

ACCEPTED MANUSCRIPT

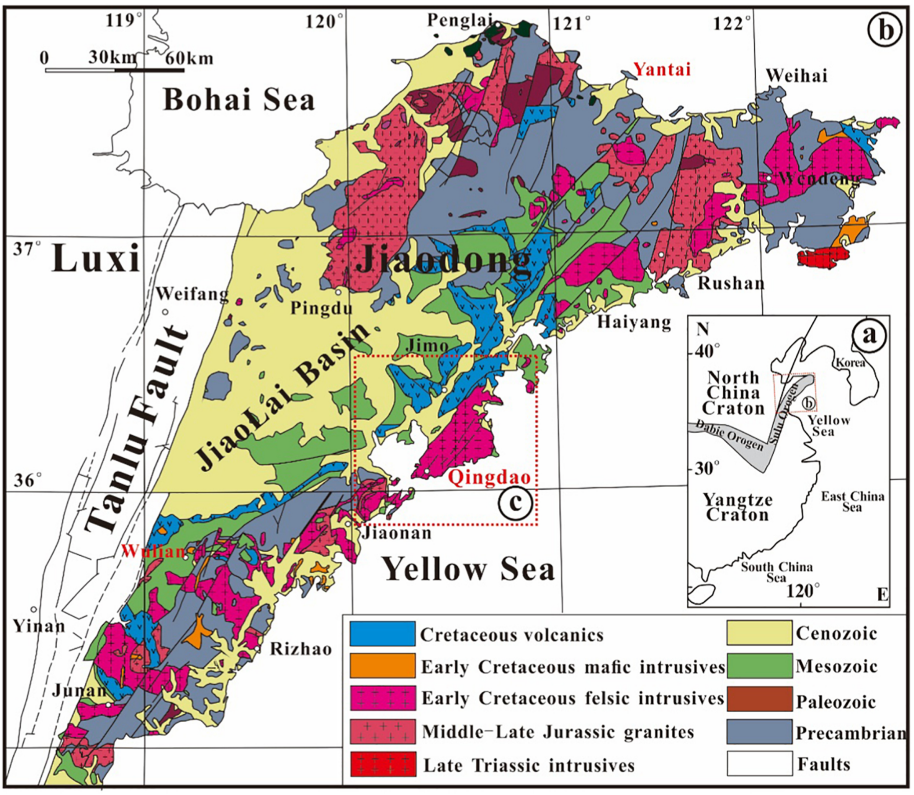
b
119°
120°
121°
122°
0 30km 60km
Penglai
Yantai
Weihai
Bohai Sea
Wendeng
37°
Luxi
Jiaodong
Weifang
Pingdu
Rushan
Haiyang
Tanlu Fault
JiaoLai Basin
Jimo
a
N
40°
Korea
North China Craton
Yellow Sea
Dabie Orogen
Sulu Orogen
30°
Yangtze Craton
East China Sea
South China Sea
120°
E
36°
Qingdao
c
Jiaonan
Weifang
Yellow Sea
Yinan
Rizhao
Junan
Cretaceous volcanics
Early Cretaceous mafic intrusives
Early Cretaceous felsic intrusives
Middle–Late Jurassic granites
Late Triassic intrusives
Cenozoic
Mesozoic
Paleozoic
Precambrian
Faults

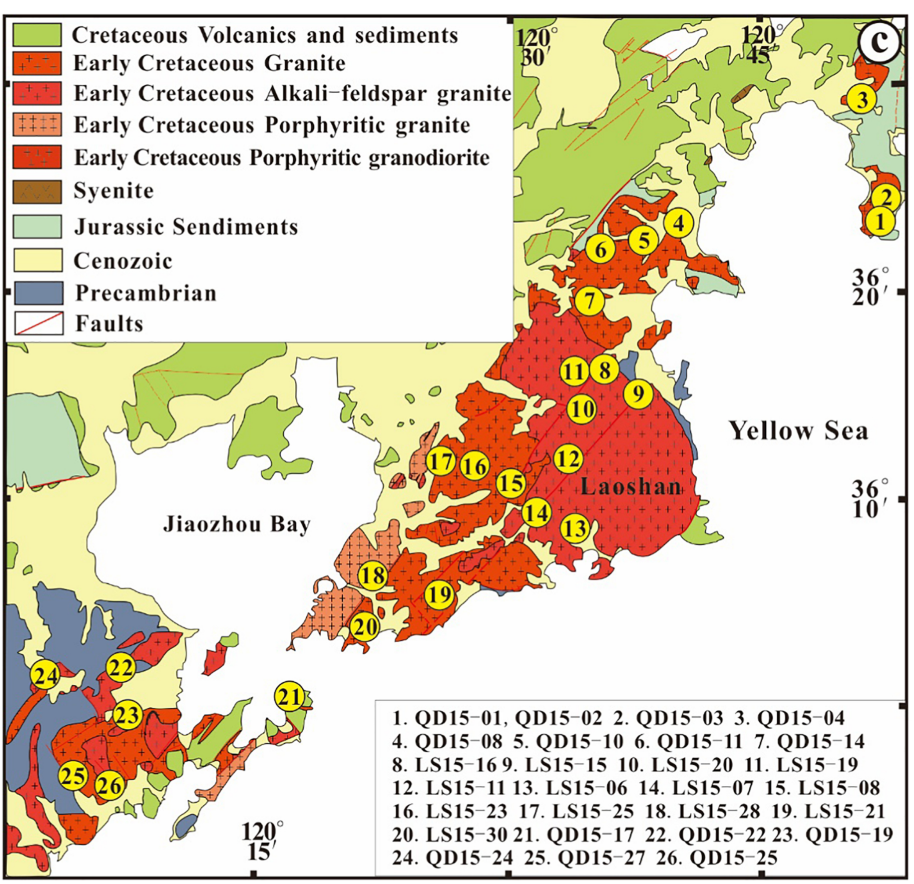
Cretaceous Volcanics and sediments
Early Cretaceous Granite
Early Cretaceous Alkali–feldspar granite
Early Cretaceous Porphyritic granite
Early Cretaceous Porphyritic granodiorite
Syenite
Jurassic Sendiments
Cenozoic
Precambrian
Faults
120° 30′
120° 45′
c
36° 20′
Yellow Sea
Laoshan
36° 10′
Jiaozhou Bay
120° 15′
1. QD15–01, QD15–02 2. QD15–03 3. QD15–04
4. QD15–08 5. QD15–10 6. QD15–11 7. QD15–14
8. LS15–16 9. LS15–15 10. LS15–20 11. LS15–19
12. LS15–11 13. LS15–06 14. LS15–07 15. LS15–08
16. LS15–23 17. LS15–25 18. LS15–28 19. LS15–21
20. LS15–30 21. QD15–17 22. QD15–22 23. QD15–19
24. QD15–24 25. QD15–27 26. QD15–25

Figure 1

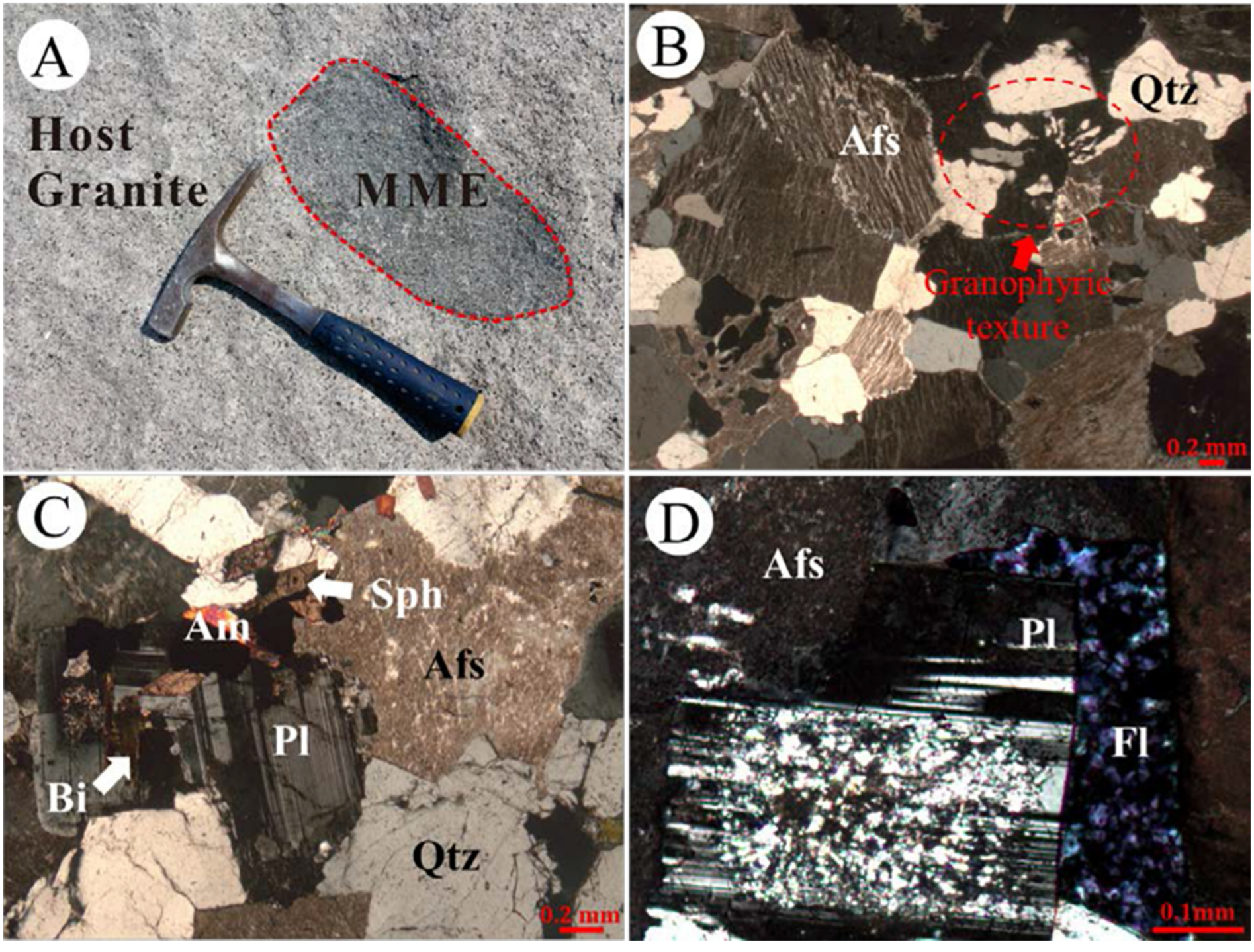
A
Host Granite
MME
B
Qtz
Afs
Granophyric texture
0.2 mm
C
Sph
An
Afs
Pl
Bi
Qtz
0.2 mm
D
Afs
Pl
Fl
0.1mm

Figure 2

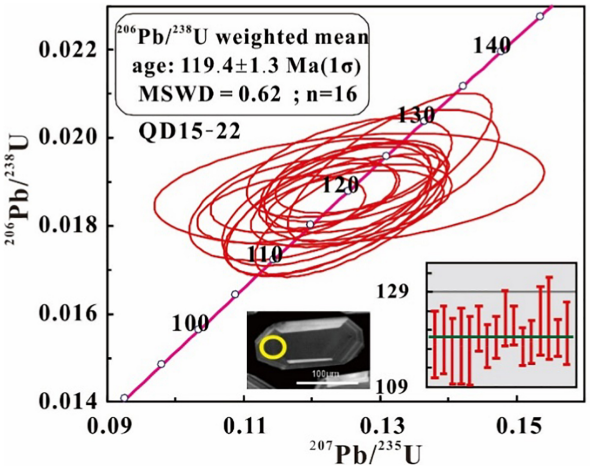
$^{206}Pb/^{238}U$ weighted mean
age: 119.4±1.3 Ma(1σ)
MSWD = 0.62 ; n=16
QD15-22
$^{206}Pb/^{238}U$
$^{207}Pb/^{235}U$
100μm

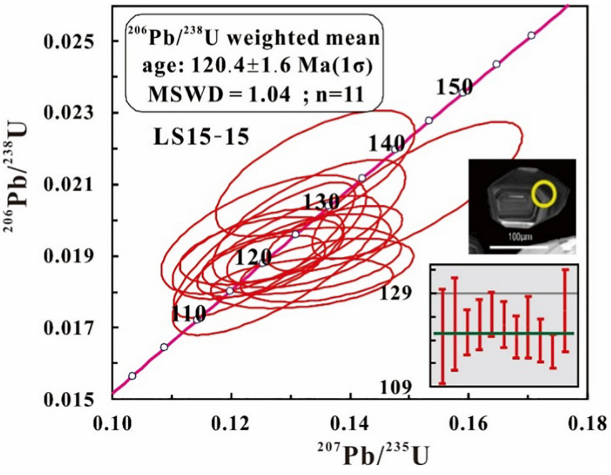
$^{206}Pb/^{238}U$ weighted mean
age: 120.4±1.6 Ma(1σ)
MSWD = 1.04 ; n=11
LS15-15
$^{206}Pb/^{238}U$
$^{207}Pb/^{235}U$
100μm

Figure 3

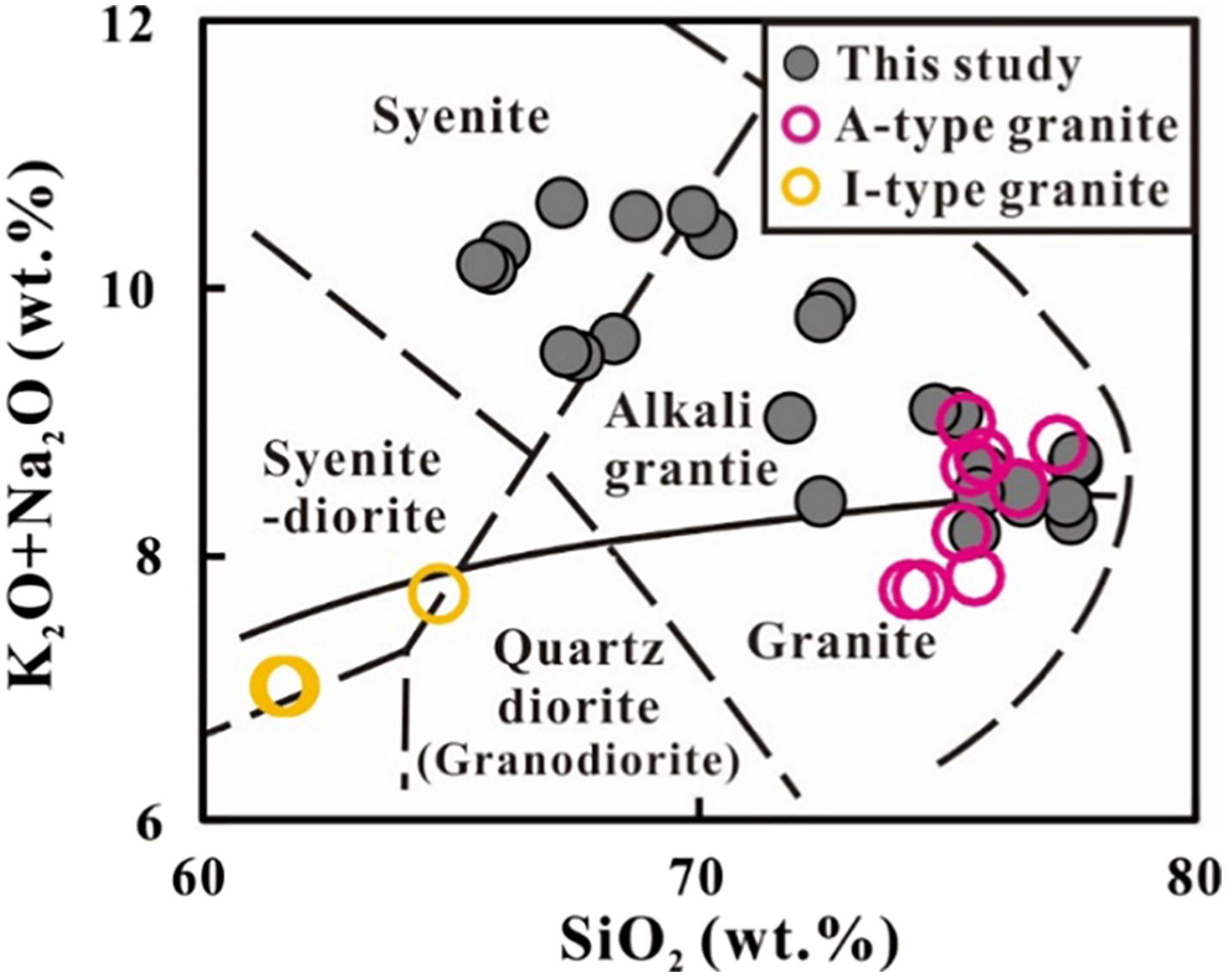
12
10
8
6
60
70
80
K_2O+Na_2O (wt.%)
SiO_2 (wt.%)
This study
A-type granite
I-type granite
Syenite
Alkali
grantie
Syenite
-diorite
Quartz
diorite
(Granodiorite)
Granite

Figure 4

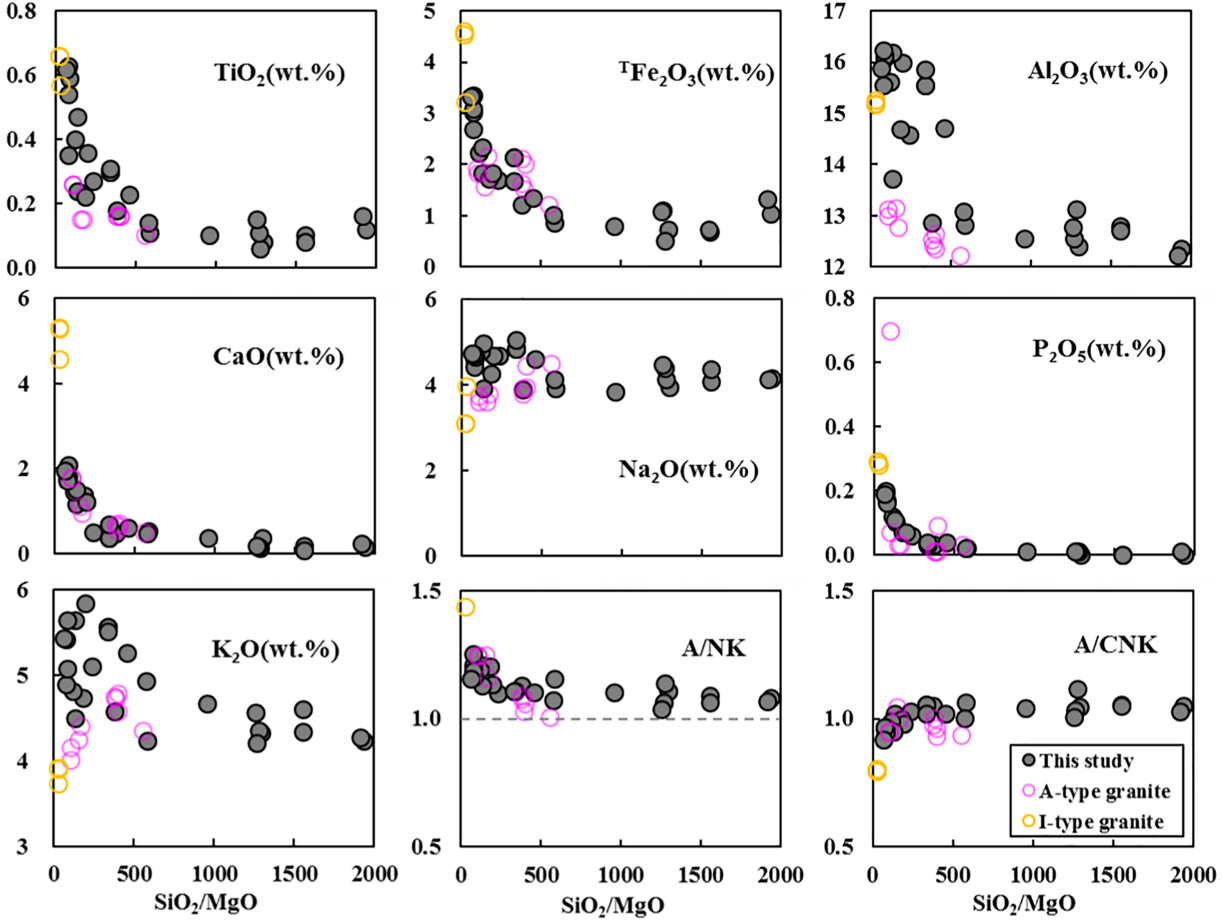
TiO2(wt.%)
TFe2O3(wt.%)
Al2O3(wt.%)
CaO(wt.%)
Na2O(wt.%)
P2O5(wt.%)
K2O(wt.%)
A/NK
A/CNK
SiO2/MgO
SiO2/MgO
SiO2/MgO
This study
A-type granite
I-type granite

Figure 5

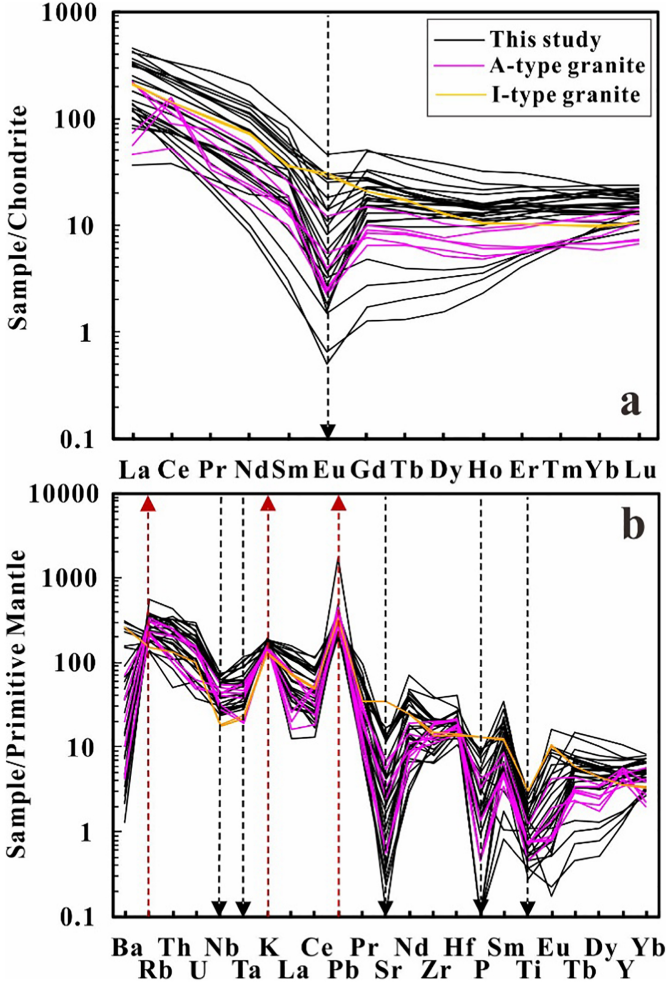
This study
A-type granite
I-type granite
Sample/Chondrite
1000
100
10
1
0.1
a
La Ce Pr Nd Sm Eu Gd Tb Dy Ho Er Tm Yb Lu
b
Sample/Primitive Mantle
10000
1000
100
10
1
0.1
Ba Th Nb K Ce Pr Nd Hf Sm Eu Dy Yb
Rb U Ta La Pb Sr Zr P Ti Tb Y

Figure 6

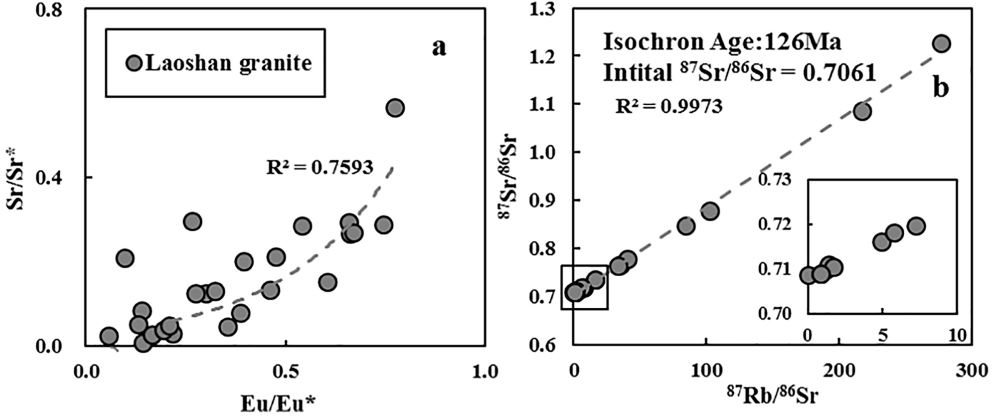
Laoshan granite
a
R² = 0.7593
Sr/Sr*
Eu/Eu*
0.8
0.4
0.0
0.0
0.5
1.0
Isochron Age:126Ma
Intital $^{87}Sr/^{86}Sr$ = 0.7061
R² = 0.9973
b
$^{87}Sr/^{86}Sr$
$^{87}Rb/^{86}Sr$
1.3
1.2
1.1
1.0
0.9
0.8
0.7
0.6
0
100
200
300
0.73
0.72
0.71
0.70
0
5
10

Figure 7

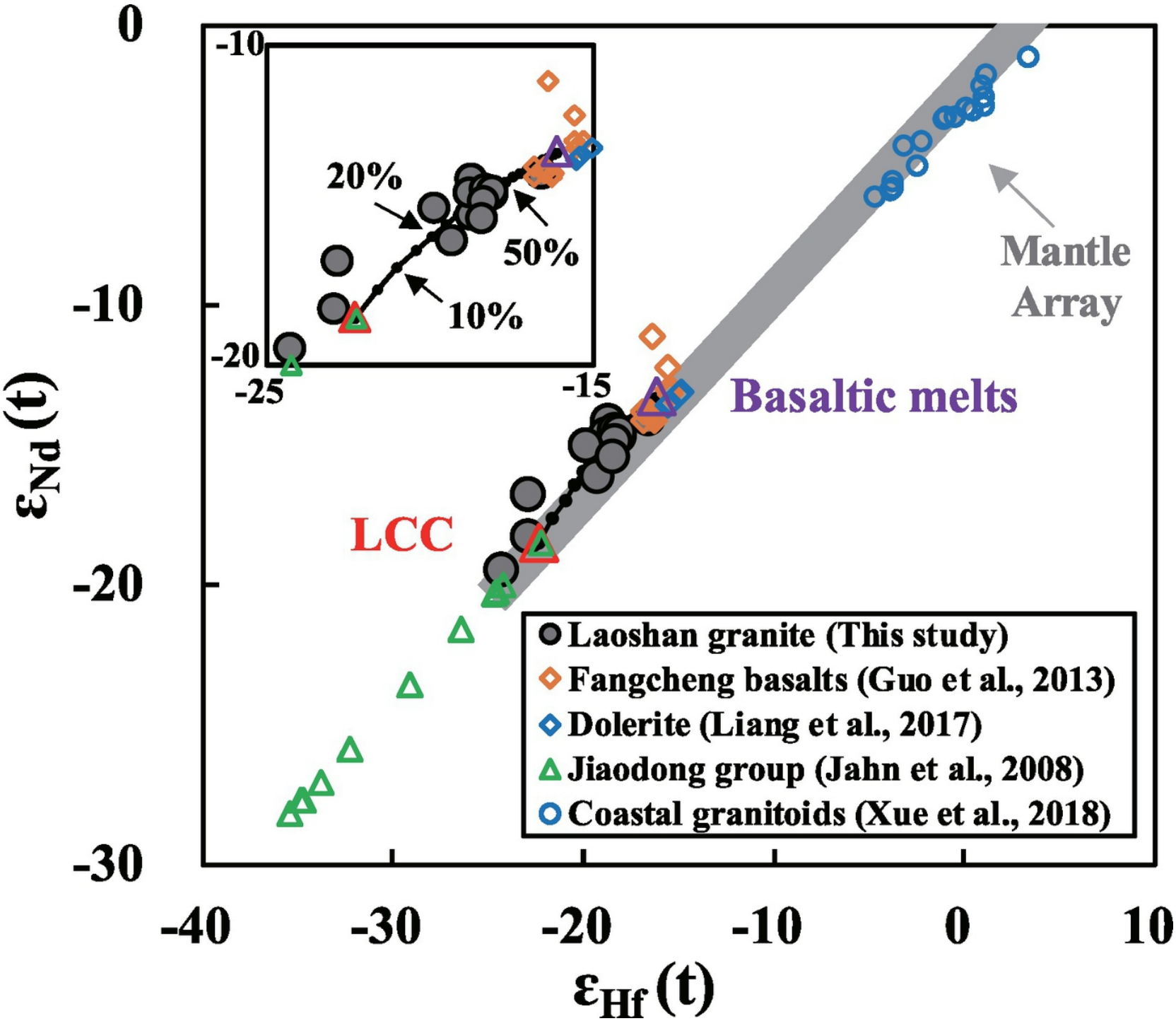
0
-10
-20
-30
-40
-30
-20
-10
0
10
$\varepsilon_{Nd}(t)$
$\varepsilon_{Hf}(t)$
-10
-20
-25
-15
20%
50%
10%
Mantle Array
Basaltic melts
LCC
Laoshan granite (This study)
Fangcheng basalts (Guo et al., 2013)
Dolerite (Liang et al., 2017)
Jiaodong group (Jahn et al., 2008)
Coastal granitoids (Xue et al., 2018)

Figure 8

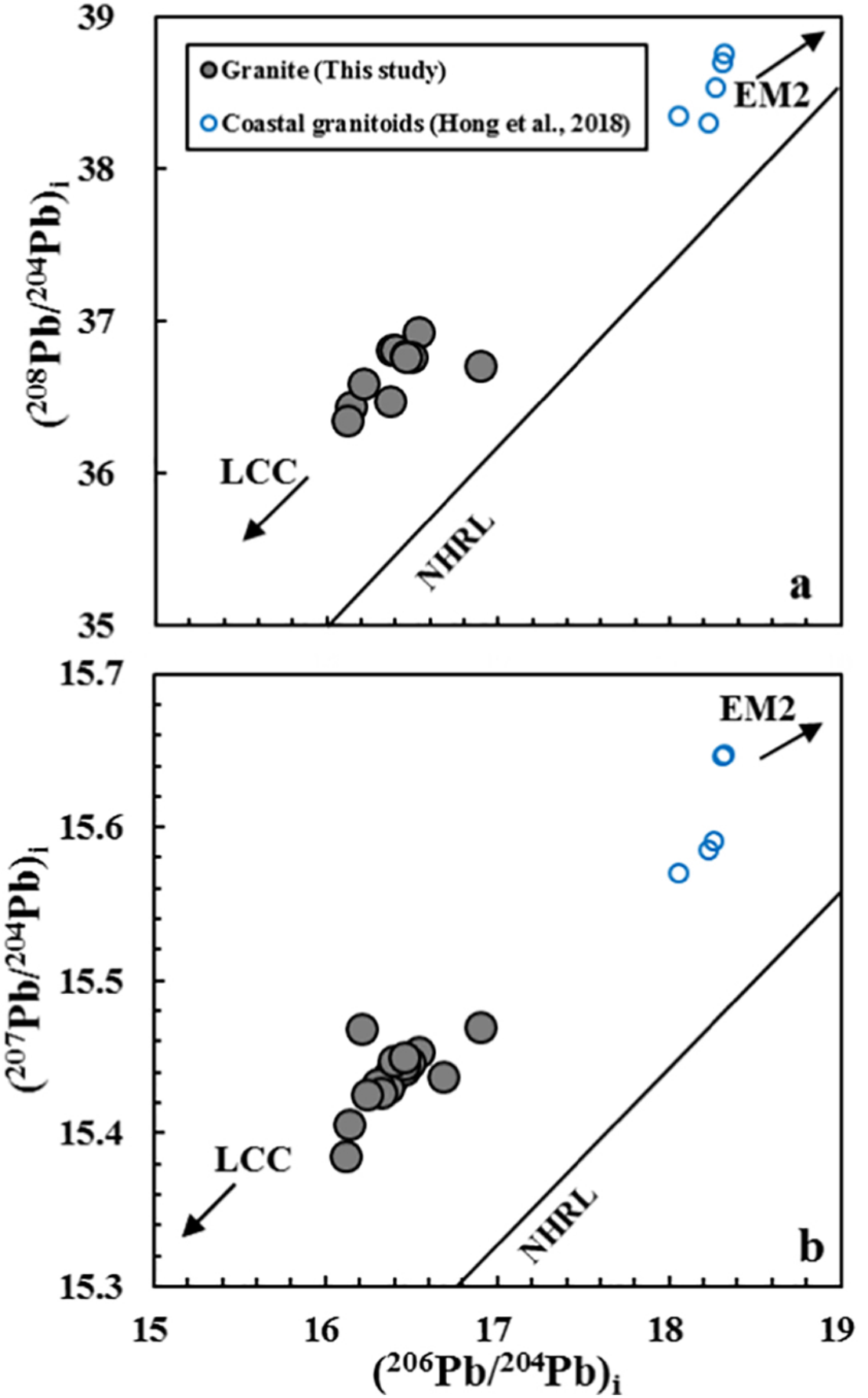
Granite (This study)
Coastal granitoids (Hong et al., 2018)
EM2
LCC
NHRL
a
b
$(^{208}Pb/^{204}Pb)_i$
$(^{207}Pb/^{204}Pb)_i$
$(^{206}Pb/^{204}Pb)_i$
39
38
37
36
35
15.7
15.6
15.5
15.4
15.3
15
16
17
18
19

Figure 9

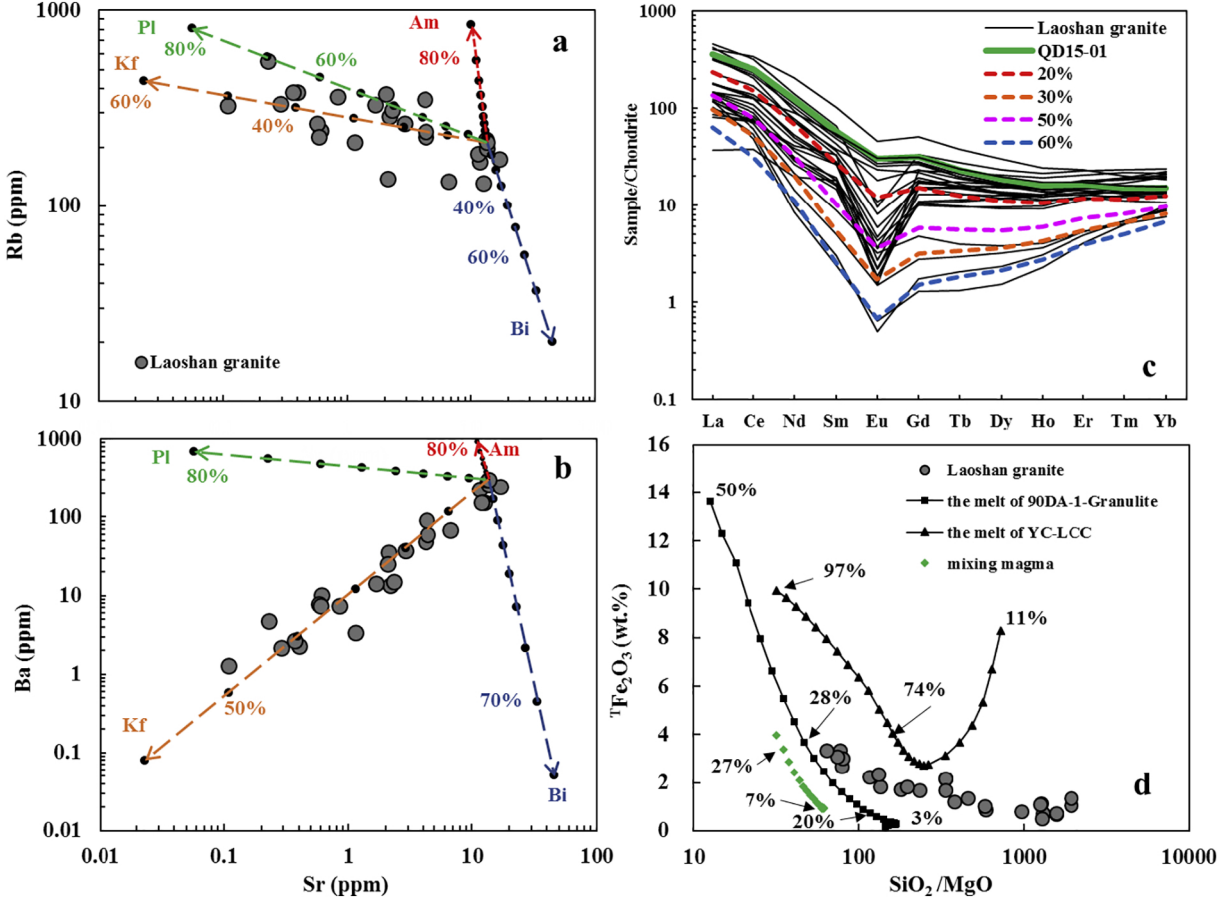
a
Pl
Kf
Am
80%
60%
40%
Bi
Laoshan granite
Rb (ppm)
b
Ba (ppm)
Sr (ppm)
c
Sample/Chondrite
Laoshan granite
QD15-01
20%
30%
50%
60%
La Ce Nd Sm Eu Gd Tb Dy Ho Er Tm Yb
d
the melt of 90DA-1-Granulite
the melt of YC-LCC
mixing magma
97%
74%
28%
11%
27%
7%
3%
Fe_2O_3 (wt.%)
SiO_2 /MgO

Figure 10

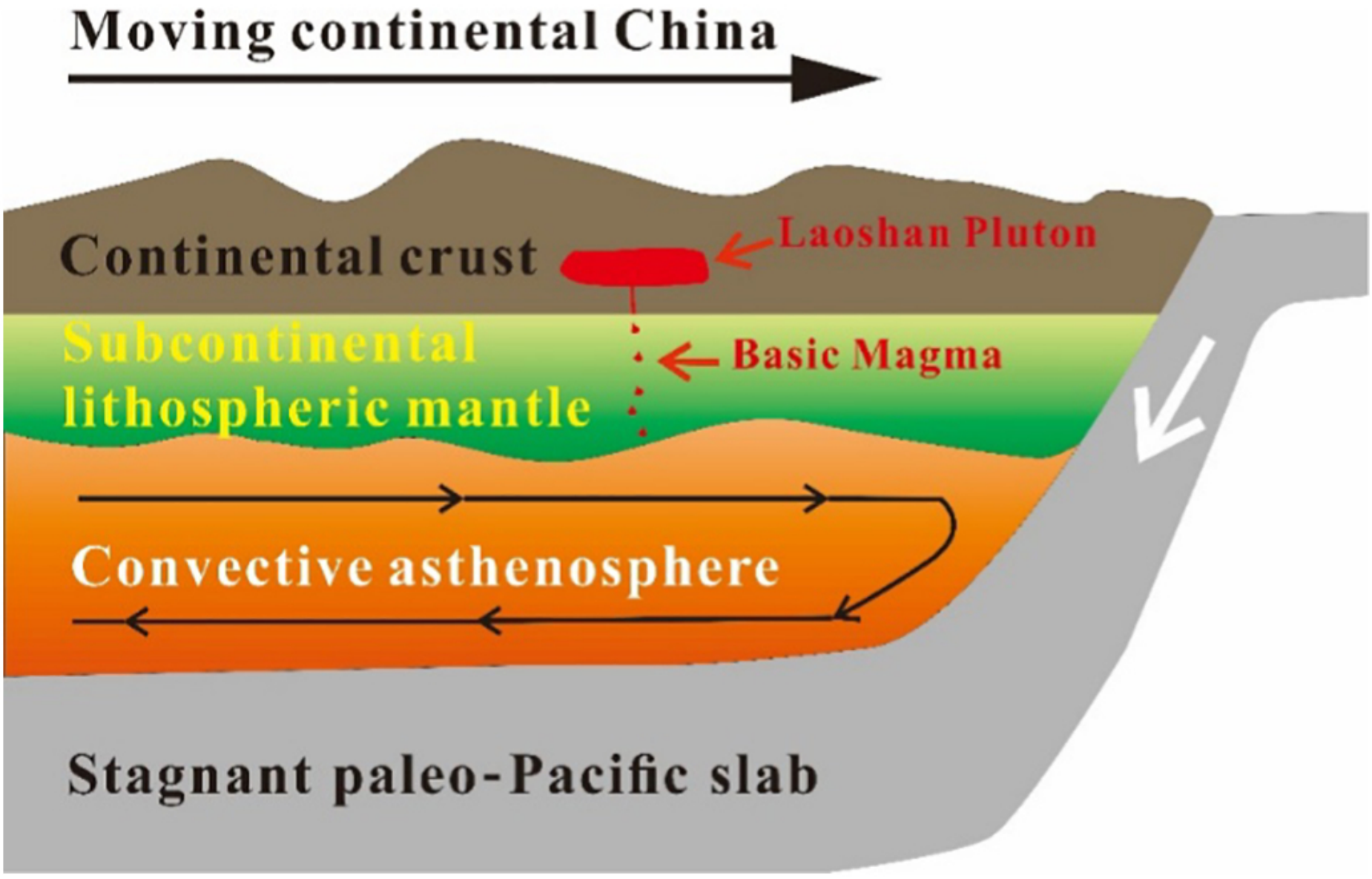
Moving continental China
Continental crust
Laoshan Pluton
Subcontinental
lithospheric mantle
Basic Magma
Convective asthenosphere
Stagnant paleo-Pacific slab

Figure 11